Direct Sensor Orientation in Airborne and Land-based Mapping Applications

by

Dorota A. Grejner-Brzezinska

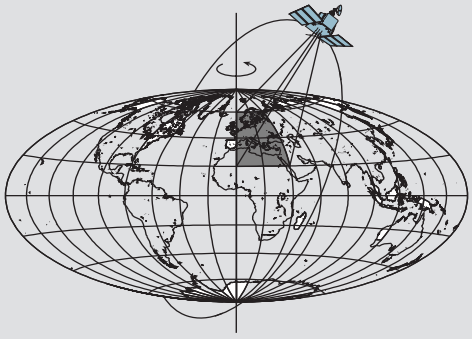

Report No. 461

Geodetic GeoInformation Science
Department of Civil and Environmental Engineering and Geodetic Science
The Ohio State University
Columbus, Ohio 43210-1275

June 2001

Direct Sensor Orientation in Airborne and Land-based Mapping Applications

by

Dorota A. Grejner-Brzezinska

Tel. 614-2928787 e-mail: dbrzezinska@osu.edu

Geodetic and Geoinformation Science
Department of Civil and Environmental Engineering and Geodetic Science
The Ohio State University
Columbus, OH 43210-1275

June 2001

Preface

The work described in this report is a summary of research and development in the area of GPS/INS (Global Positioning System/Inertial Navigation System) integration for direct georeferencing of imaging sensors to support precision airborne and land-based mapping. The research was conducted at the Ohio State University Center for Mapping and the Department of Civil and Environmental Engineering and Geodetic Science (CEEGS). The author wishes to acknowledge the following faculty and research staff, who actively participated and supported this research: Prof. John Bossler, retired director of the Center for Mapping and Professor Emeritus of CEEGS and Dr. Charles Toth, Research Scientist of the Center for Mapping. Their support and cooperation are greatly appreciated.

The work presented here was supported by the National Aeronautics and Space Administration (NASA) grant, OSU # 733223, the Ohio Department of Transportation (ODOT) grant, OSU # 733488, and the Federal Department of Transportation (FDOT) grant, OSU # 739152.

ABSTRACT

Since the early 1990s, the concept of Mobile Mapping Systems (MMS) has evolved from rather simple land-based systems to more sophisticated, real-time multi-tasking and multi-sensor systems, operational in land and airborne environments. Mobile Mapping technology has made a remarkable progress, notably expanding its use in remote sensing, and surveying and mapping markets. New systems are being developed and built for specialized applications, in support of land-based and airborne imaging sensors, aimed at automatic data acquisition for GIS databases.

The major objective of this report is to review the concept of Mobile Mapping System and GPS/INS supported direct platform orientation (DPO) in particular, as well as their evolution since early 1990s, with a special emphasis on the research and development carried out in this area at the Ohio State University. A short review of the inertial navigation concept is given, and a notion of GPS/INS (inertial navigation system) integration is also presented. The concept of direct georeferencing is also explained and compared to the traditional aerotriangulation (AT) method of image geo-registration, and the importance of multi-sensor system calibration is discussed, including its impact on the positioning accuracy. Some examples of currently attainable navigation performance, based on the OSU-developed Airborne Integrated Mapping System (AIMS) and the land-based system for highway mapping are discussed, and future perspectives of MMS are presented.

Although MMS may be, in general, associated with land-based applications, the concept of airborne mapping (remote sensing) based on DPO is also discussed here, primarily due to the fact that airborne positioning and orientation systems based on GPS/INS integration are based on similar hardware and software designs, and clearly evolved from the traditional airborne mapping as a consequence of the advent of a high-accuracy GPS/INS systems. Thus, the DPO facilitated through GPS/INS fusion is a common denominator for the modern land-based and airborne mapping, which often times involves multiple imaging sensors to achieve higher accuracy, and data complementarity and redundancy.

KEYWORDS: mobile mapping, direct georeferencing, GPS/INS integration, multi-sensor systems

1. INTRODUCTION

A Mobile Mapping System (MMS) can be defined as kinematic platform, upon which multiple sensors have been integrated and synchronized to a common time base, to provide three-dimensional near-continuous and automatic positioning of both the platform and simultaneously collected geo-spatial data. MMSs are most commonly designed as modular systems that can be installed on various land or airborne platforms, and their components can be easily replaced by more advanced counterparts as technology progresses. The primary components of MMS are (1) the control module, (2) the positioning module, (3) the imaging module, and (4) data post-processing module, creating together a multi-tasking system, capable of handling numerous concurrent operations in real-time (and post-processing mode), providing automatic acquisition of directly oriented (georeferenced) digital imagery for mapping and GIS data collection.

The direct georeferencing, also referred to as direct platform orientation, DPO, is usually facilitated by the integration of Global Positioning System (GPS) in a differential mode and an Inertial Navigation System (INS), providing high-accuracy positioning and attitude information of the imaging sensor(s). While land-based MMS, usually driven at normal speeds, travels on a highway, city or a state road, the GPS/INS module collects positioning and attitude information of the image acquisition events. Real-time or post-processing of these data provides directly georeferenced stereo-pairs (or multiple stereo-pairs per epoch if more than two cameras are used) in a selected mapping coordinate system. Oriented images are then used in a photogrammetric processing to extract the feature data together with their positional information. Features and additional attributes acquired this way can be directly transported to a GIS database, or converted to a digital map. Since data acquisition represents one of the most expensive (if not the most expensive) components of establishing a GIS database, the MMS concept was developed with a primary focus on automation and acceleration of the data capture process. Even to date, many land-related databases still rely on the existing maps, which are digitized to provide necessary information and attributes. Thus, by introducing MMS technology, fully based on directly georeferenced multiple digital imaging sensors, the time of data capture has been indeed dramatically decreased, while the quality of positioning information increased significantly with respect to accuracy of the topographic maps traditionally used.

The concept of Mobile Mapping System dates back to late 1980s and early 1990s, when the Ohio State University Center for Mapping initiated the development of GPSVan™ – a first land-based mapping system designed to automate and speed up the collection of direct digital imagery (Bossler et al, 1991; He and Novak, 1992; Bossler and Novak, 1993; He at al, 1994, Bossler and Toth, 1995; Novak and Bossler, 1995; Toth, 1995a; Grejner-Brzezinska, 1996). At the same time, the University of Calgary started a joint project with GEOFIT Inc., aimed at the development of VISAT system designed for mobile highway mapping (Schwarz et al, 1993; El-Sheimy et al, 1995 and 1995b; El-Sheimy and Schwarz, 1999). By mid-1990s more systems, based on similar concept, have been under development, among them GPSVision by Lambda Tech International, Inc (He et al, 1996). Moreover, with proliferation of GPS/INS technology, DPO airborne systems development followed, and by mid-1990 several systems and applications, based on all digital, GPS/INS georeferenced imagery, were reported (see for example, Schwarz et

al., 1993; Kerr, 1994; Lithopoulos et al., 1996; Abdullah, 1997; Da, 1997; Grejner-Brzezinska, 1997). Major existing land-based mobile mapping systems are listed in Table 1 below.

Table 1. Overview of the existing mobile mapping systems (partially shown in Li et al., 1999).

MM System	Development Institution	Navigation Sensors	Mapping Sensors
GPSVan™	Center for Mapping, OSU	GPS/Gyro/Wheel Counter GPS/INS (second generation of the system)	2CCD, voice recorder
VISAT	University of Calgary	GPS/INS/ABS	8 b/w CCD and 1 color SVHS
GeoVan	Geospan Corp., USA	GPS/DR	10 VHS, voice recorder
GPS Vision	Lambda Tech. Inc., USA	GPS/INS	2 color CCD
KISS	Univ. of Bundeswher Munich and GeoDigital, Germany	GPS/IMU/Inclination Odometer/Barometer	1 SVHS, 2 b/w CCD, voice recorder
ON-SIGHT	Transmap Corp., USA	GPS/INS	4 color CCD
RGIAS	Rowe Surveying and Eng., Inc., USA	GPS	video, laser range finder
TruckMap	John E. Chance Inc., USA	GPS/Gyro/WADGPS	Laser range finder, 1 video camera
WUMMS	Wuhan University, China	GPS	3 video cameras, laser range finder
ROMDAS	Highway and Traffic Consultants Ltd., New Zealand	GPS	digital video camera
DDTI	Digital Data Technologies, Inc., USA	GPS	touch-screen, voice recorder
POS/LV^{TM} 420	Applanix Corporation, Canada	GPS/INS/ distance measuring instrument (DMI)/ GPS Azimuth Measurement Subsystem (GAMS)	CCD, video

In this contribution, a review of MMS operational principles, its major components and implementation aspects are presented. Special emphasis is put on GPS/INS integration, modern imaging sensors and the comparison of direct vs. traditional methods of georeferencing. The multi-sensor system calibration, achievable accuracy and future perspective, as well as examples of the existing integrated land-based and airborne mapping systems are also discussed.

2. MOBILE MAPING SYSTEMS: OPERATIONAL PRINCIPLES

A typical land-based modern MMS is presented in Figure 1. This particular system represents a second generation of GPSVan™ — a first mobile mapping system developed by the Center for Mapping and licensed to Transmap Inc[1]. An example of the Airborne Integrated Mapping System, AIMS™, also developed at the Center for Mapping, is illustrated in Figure 2 (Bossler and Schmidley, 1997; Da, 1997; Grejner-Brzezinska, 1997; Grejner-Brzezinska et al, 1998; Toth, 1998).

2.1. Major components of MMS

The primary components that constitute a mobile mapping system are differential GPS, INS and imaging sensor(s). Generally, multiple cameras (directly oriented by GPS/INS) are mounted on the top of a land vehicle for stereo vision and full directional coverage, while single down-looking camera is the most common imaging sensor configuration in airborne systems. The stereovision system, as presented in Figure 1, provides 3D measuring tools to obtain object coordinates without object space control. Two forward and two backward looking cameras, capturing image pairs, are mounted on fixed bases, which establish the model scale. The relative positions and orientation of cameras are constant (following system calibration, see Section 7), thus 3D spatial coordinates can be computed in a local coordinate system attached to the left camera, while the final object coordinates can be determined by connecting this system to the positioning (mapping) system of the navigation component (GPS/INS). Imaging plays an important role in MMS, connecting the moving platform to the environment to be mapped. Features are identified in the images and their coordinates are derived from the positioning information of the vehicle. Due to the storage problems, early MMS were equipped with analog video systems. Following significant advancements in storage technology (from the tape systems, to magnetic disks and currently — to more advanced, rather compact and rugged magnetic disks (disk arrays), capable of storing large amounts of data, and sustaining data rate of 40-50MB/s), fully digital cameras have become an inherent part of mobile mapping, allowing for even more automation of the data processing. It should be mentioned here that with recent technological advances, multiple imaging sensors, such as CCD-based (Charge-Couple Device) cameras and LIDAR (Light Detection and Ranging), are often mounted on the same airborne platform to support multi-purpose geospatial data collection.

A minimum of two GPS receivers — a static base and a mobile rover, virtually attached to the independent INS unit, are intrinsic parts of any MMS, forming a positioning/attitude module of the system. Commonly, two static base stations are established for quality control and more robust solution. Independent ground control points are usually established (or existing control is utilized) to provide separate quality measures. Typically, the expected positional accuracy with a 2-meter camera base is in the order of 10-20 cm for a fully calibrated system with object distances between 5 and 20 m (He et al., 1994). Although the positioning data processing is

[1] Transmap Inc., established in 1994 carried forward a successful commercialization of GPSVan™ technology, now redesigned, modernized and fully automated, implemented on several vehicles, serves mapping needs of the government and private industry.

performed in WGS84, which is a GPS reference system, individual horizontal and vertical datum, as well as commonly used map projections are inherently built in the overall data processing flow, providing the user with the final feature-positioning results in a selected reference mapping frame. A PC onboard a mobile mapping system provides the system integration and control support, as well as a storage media and a display for the operator's interaction during the data acquisition. If the system is designed for real-time operation, a radio connection must be established with the GPS base station for RTK GPS. Systems based on DGPS services must be capable of receiving radio-navigational beacons and/or satellite-based differential signal (such as OmniStar).

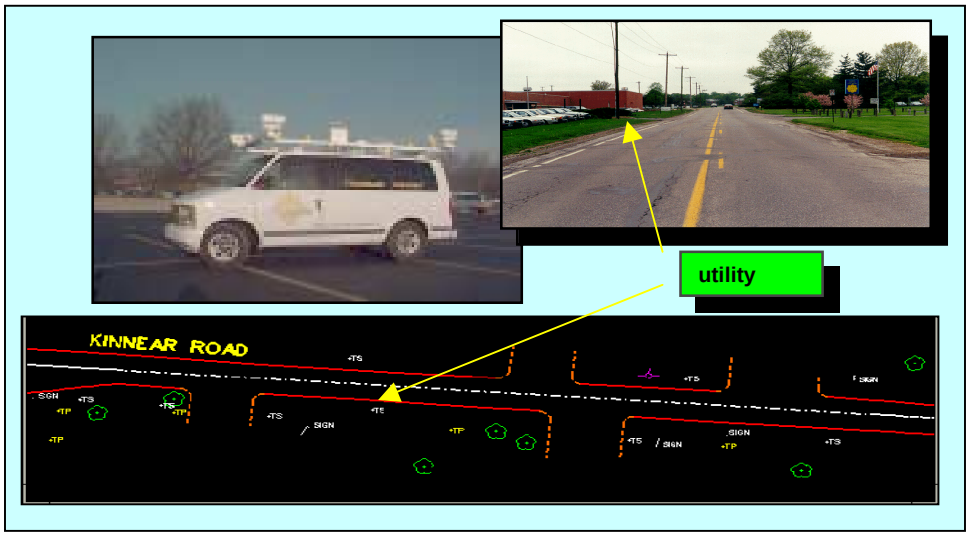

Figure 1. Mobile mapping system specialized for highway and railroad inventory surveys (courtesy of Transmap Inc.)

Major Operational Components of MMS:

- System calibration (performed after the system has bee mounted in the vehicle)
  - GPS/INS lever arm (offsets between the GPS antenna phase center and the center of the INS body frame)
  - Camera calibration
  - INS/camera boresight calibration (linear and angular offsets between the INS and the camera and body frames)
- GPS/INS/image data collection
  - GPS/INS/camera time synchronization
  - Data logging
  - Image compression and storage
- GPS/INS post-processing for six exterior orientation parameters (time-tagged image registration to the navigation system positioning results)
- Image processing on a softcopy system (georeferenced images are used for feature location; for less demanding application monoscopic image processing suffice; when high accuracy is required, stereo imagery and restitution must be used)

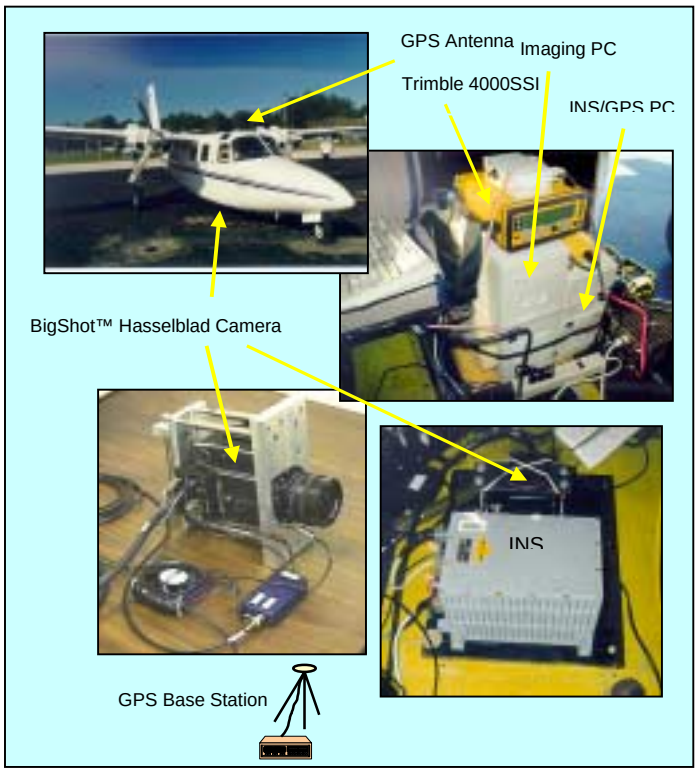

Figure 2. The Airborne Integrated Mapping System AIMS™.

Table 2. Primary sensors of MMS and their functionality.

Primary sensor	Sensor Functionality
GPS	• Image geo-positioning in 3D • Time synchronization between GPS and INS • Image time-tagging • INS error control • Furnishes access to the 3D mapping frame through WGS84
INS	• Image orientation in 3D • Supports image georeferencing o Provides bridging of GPS gaps o Provides continuous (256Hz) trajectory between the GPS measurement epochs • Supports ambiguity resolution after losses of lock, and cycle slip detection and fixing
Camera	• Collects imagery used to derive object position o Two (or more) cameras provide 3D coordinates in space o Single camera provides 2D coordinates or 3D if overlapping images are used
Laser Range Finder	• Supports feature extraction from the imagery by providing precise distance (typical measuring accuracy is about 2-5 mm)
Voice recording, touch-screen, barometers, gravity gauges	• Attribute collecting sensors

2.2. Why is precise timing so important?

A factor, crucial for achieving high accuracy positioning, based on multi-sensor system integration, is precise time synchronization, usually realized by the exchange of synchronization signals, which relate different sensors to a common time frame provided by GPS. By design, GPS provides an excellent time reference, offering a foundation for any timing tasks. Similarly to GPS, the INS systems also come with an integrated timing module. However, it normally works in a free-run mode and is very rarely directly synchronized to UTC (Universal Coordinated Time – basis for most radio time signals and legal time systems, based on the atomic second, thus its rate is uniform; its epoch is manipulated accordingly, so that the difference between UT1 (rotational time) and UTC is maintained on a level less than or equal to 0.7 s. For that purpose UTC is modified by introducing a leap second, when required, e.g., on December 31 and/or June 30. GPS time, also based on the atomic second, is now ahead of UTC by 13 seconds). In MMS, the internal timing unit of the INS system must usually be synchronized to the GPS clock during initialization, and can also be calibrated for possible scale errors (clock drift) in the post-processing. Commonly used hardware platforms, providing universal timing functions are commercially available multi-channel timing boards. A quality timer unit can deliver 1-μs resolution, and its counters can be synchronized to 1 PPS GPS signal. The absolute accuracy of a good timing board clock could be calibrated to about 0.2%, and the stability is around 1 PPM. Our earlier tests with DOS-based systems (Toth, 1998; Grejner-Brzezinska et al., 1998) have shown that 5-10 μs response times are achievable for very high event rates (1000 events/s). This timing error translates only into 1-2 mm error at 200 m/s platform speed. Both the imaging events and the INS data records are timed by the timing board clock, synchronized to the GPS time, as described above. It should also be mentioned here, that the optional built-in timer in GPS receivers could also provide a reliable support for the timing requirement of photogrammetric cameras. However, additional timing devices should always be used in more demanding applications, especially, when very high sampling rate is used (i.e., INS data acquisition in MMS).

2.3. Multi-sensor system: a state-of-the-art MMS

Clearly, modern airborne and land-based mapping technology represents a class of multi-sensor systems, combining GPS/INS-based navigation module with the single or multiple-sensor image module. Multi-sensor systems that combine direct positioning and imaging sensors are rapidly becoming a standard source of information for various aerial mapping applications including surface reconstruction. An optimal fusion of multi-sensory data, supported by geometric fusion (time-space registration) facilitated by GPS/INS, brings together complementary and often redundant information, as sensors based on different physical principles register different properties of objects. This, in turn, translates to a more consistent scene description enabling an improved scene interpretation/understanding. Thus multi-sensor systems provide complementary, fast, accurate, fault-resistant and cost-effective data that can be used in a variety of mapping tasks. For example, frame cameras and Laser (Light) Detection and Ranging (LADAR or LIDAR) are the most commonly used imaging sensors, providing data for surface and elevation model generation. Traditional photogrammetric methods, based on stereo panchromatic frame imagery, are well established and have been widely available in commercial off-the-shelf

software packages. Airborne laser ranging (ALR) systems that employ a laser-scanning device represent, on the other hand, a relatively new method of surface data acquisition. Moreover, the ALR processing techniques are still far from being fully developed, and at this point only very specialized or even experimental software packages are available.

3. WHAT ARE THE MAJOR BENEFITS?

Since the inception of the mobile mapping technology, the concept of direct georeferencing (with virtually no or very limited ground control and no need for aerial triangulation, AT) based on multi-sensor mapping systems has become of increasing interest to the mapping and remote sensing communities, driven primarily by the cost-effectiveness, automation and optimization of data flow, and short turn-around time (see Figure 3 for comparison of traditional and all-digital directly-oriented aerial mapping).

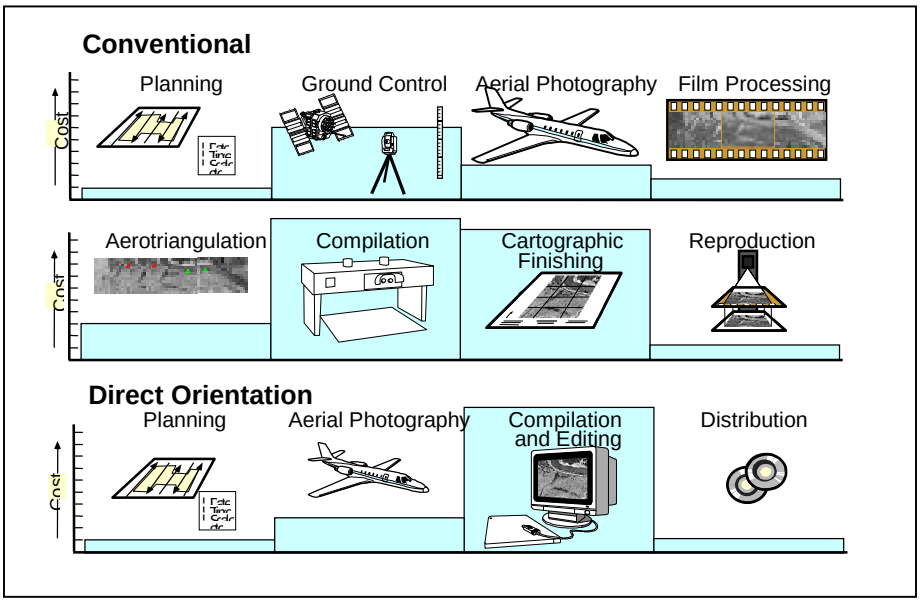

Figure 3. Cost comparison between the conventional and DPO–based aerial mapping.

Long-time users of MMS technology in the land-based highway corridor mapping emphasize the following benefits: estimated 10:1 saving in data collection, estimated 10:1 reduction in field trips, pro-active maintenance of assets, improved service and increased productivity. While mapping and surveying market is strongly fragmented and undercapitalized, based largely on government contracts and having substantially long sales cycles, mobile mapping technology certainly brings new, economically attractive solution to virtually all mapping needs. Bearing in mind that the GIS and mapping market represents one of the most dynamically growing geo-industries (currently worth over 8.2 billion US dollars worldwide, with $500 million mapping market and 30% annual growth), it is perhaps safe to predict that fast and effective technologies, such as MMS, will further continue their growth.

It must be emphasized here, however, that despite their attractive characteristics in terms of image quality and short processing time (no film development), modern digital cameras with

their limited footprint (see Section 4) might impose some limitations on airborne or space borne mapping applications (as opposed to using large-format analog cameras). Specifically, the use of a 3" by 3" digital sensor, instead of 9" by 9" film, would result in nine times as many images. With this number of images, performing a traditional AT-based project, one would have to accept an increase in the number of point measurements approximately by one order of magnitude, which obviously is unacceptable from the production viewpoint. Having GPS/INS-based DPO data, however, can reduce the processing cost and time, making the number of images practically irrelevant. In that sense, further advancements in GPS/INS systems might prove crucial to the development of airborne digital cameras and their upcoming introduction to the airborne surveying market. For the line sensors, which offer larger ground coverage, the need for GPS/INS is even more important since otherwise, the reconstruction of the geometry for airborne platforms is almost impossible (every scan line requires an independent set of DPOs).

4. MODERN IMAGING SENSOR IN MMS AND REMOTE SENSING

It is beyond the scope of this paper to provide a full analysis of digital sensors available on the market and used in various mapping applications (a good review is presented by Toth, 1999). However, since the imaging module is an intrinsic component of any mobile mapping system, a brief discussion related to two, perhaps most important and commonly used sensors in MMS and airborne remote sensing, digital frame cameras and LIDAR, is presented in this section. It is worthwhile to mention here that even though the mobile mapping was first defined as a land-based system, the aerial platforms using modern GPS/INS-based georeferencing technology as well as emerging imaging sensors, including LIDAR, are considered state-of-the-art airborne mobile mapping technology. Therefore, a brief discussion presented here includes LIDAR, predominantly used by the airborne system for fast and accurate elevation data capture.

4.1. Digital cameras

Before exploring the mapping market, the digital imaging systems have been widely used in non-mapping applications for over two decades. The first CCD-based sensors used in airborne/space born mapping were linear arrays, even though the use of linear imaging sensors in mapping is rather difficult from a photogrammetric data processing viewpoint, since the orientation of every image line requires robust modeling of the sensor trajectory. On the other hand, the area CCD-based systems are fully compatible with the standard frame camera model, and thus, easily fit current map-production practice, therefore these sensors (providing smaller image size as compared to the scanning devices) have been primarily used in land-based mobile mapping systems. In the mid-90's, when advances in semiconductor technology enabled manufacturing of larger CCDs area sensors with 4K by 4K up to 8K by 8K pixels have become more common, and by the end of the past decade were used rather routinely (Bruce 1998; Pfister et al. 1998; Toth, 1999). Examples of two high-end CCD-based cameras are shown in Figures 4 and 5.

Majority of currently available CCDs are rather limited in size (see Table 3 for high-end systems), offering not more than one-fourth of the image size of a traditional aerial camera. Nevertheless, this size constraint is not very critical for airborne applications such as corridor mapping, where the swath width is relatively small. Furthermore, electronic imaging is a

precondition for any real-time application offering at the same time a clear advantage over analog film-based techniques by substantially reducing turnaround time and providing easy connection to softcopy systems. Moreover, assuming obvious benefits from direct orientation, and thus, no need for aerial triangulation (except for calibration and quality control, QC), the smaller image size does not create any problems to the feature extraction process in a softcopy environment. It should be mentioned here that the use of the new, 6" silicon wafer, although still in the experimental phase, promises to further increase the active sensor area, offering already a 10K by 5K CCD (Pfister et al. 1998).

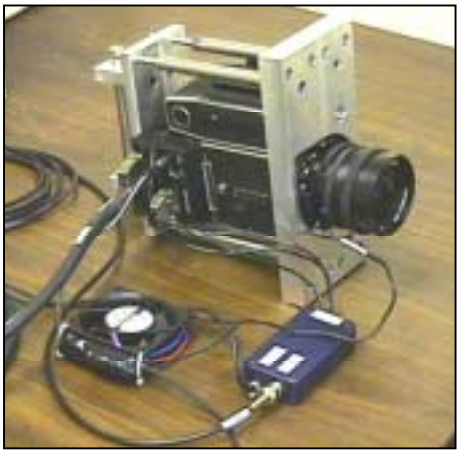

Figure 4. Lockheed Martin Fairchild BigShot™ with Hasselblad 553 ELX camera body.

Figure 5. Kodak Megaplus ES 1.0/MV digital camera.

Table 3. Frame CCD currently available on the market (Toth, 1999)

Manufacturer	Model	Array Size [H x V]	Pixel Size [micron]	Data Rate [MHz]
Kodak	DCS-460	3,072 x 2,048	9	10
Lockheed Martin	BigShot™	4,096 x 4,096	15	5
Kodak	Megaplus 16.8i	4096 x 4096	9	10
Philips	Icam28	7,168 x 4,096	12	18
Recon/Optical/Dalsa	CA-260/50	10,080 x 5,040	10	48/64
Lockheed Martin	F-979F	9,216 x 9,216	8.75	160

Recent developments in storage and compression technology have reached the point where digital imagery can quite effectively compete with analog, film-based techniques in applications like MMS and even aerial photography. Moreover, the small size (1K by 1K to 2K by 2K) CCD-based technology (used in land applications) is very well established, providing virtually flawless chips, electronic shutters, color or b/w options, and very fast (up to video) output rates. The fully digital workflow offers numerous advantages, such as improved triggering, low noise level, no

signal corruption during storage, and requirements for digitization. Also, several real-time processing tasks are possible while using digital imagery. Those include (Toth, 1995b):

- Signal conditioning (gain and offset control, color corrections)
- Image enhancements (real-time histogram collection and correction)
- Imprinting (equivalent to titling in the analog case)
- Image compression

Some other properties that, besides a smaller sensor size, clearly distinguish frame CCD arrays from analog film include (Toth, 1999):

- Manufacturing of flawless CCDs (with over ten million pixels!) is practically impossible. However, the location of bad pixels is known and is available to the users, allowing the replacement of the bad pixel intensity with some interpolated value.
- The time it takes to shift out all the pixels from a CCD (read-out rate) can be quite substantial, reaching a few seconds (especially in the older systems), which can considerably affect the flight plan (especially the flight speed). Newer systems, usually based on multiple output gates, offer significantly increased read-out rate.
- In contrast to analog film, CCDs have a linear characteristic and thus are much more subject to saturation (blooming), causing a charge spill over from the saturated pixels to neighboring pixels.
- The radiometric sensitivity of CCDs is around the 100-200 ASA or higher.
- CCDs, especially cooled ones, can exhibit very good signal-to-noise ratios and can therefore typically produce pixel intensities with 10-12 bit resolution, much better than the currently realized 6-7 bit intensity resolution of scanned analog imagery.

New digital imaging systems for airborne photogrammetry are being developed, and the digital market becomes more and more competitive, with major players such as Z/I Imaging and LH Systems entering the market. Both companies announced their new products at the ISPRS Congress in Amsterdam in July 2000. The Z/I Imaging Digital Modular Camera (DMC) is based on the 4096 x 4096 Kodak chip listed in Table 3, where more than one individual camera module can be tied together, resulting in a large field of view of the camera. The fully-equipped configuration of the DMC is composed of four panchromatic modules (4K by 4K each) and up to four multi-spectral channels, and a post-processing procedure ("mosaicing") is used to transform the four individual images into one virtual image considered as normal central projection (Diener et al., 2000). The LH Systems ADS40 airborne digital sensor offers a modular design, based on three panchromatic and four multi-spectral CCD lines. The three panchromatic sensor lines produce the forward, nadir and backward views along the strip. Each panchromatic line consists of two linear arrays, each with 12000 pixels, staggered by 0.5 pixels. Each sensor line is measured during camera calibration so that the precise position of each pixel on the focal plane is known (Reulke et al., 2000; Sandau et al., 2000).

4.2. Airborne laser ranging (ALR)

First experimental applications of ALR date back to the 1970s and 1980s. However, this technology was first introduced to the mapping community about a decade ago. Recently, the technology's maturity and also rapid development of the GPS/INS direct orientation systems supporting ALR, has increased interest in the laser-based systems. There exist several operational LIDAR topographic systems, manufactured either as proprietary or commercially available systems; examples are: Azimuth Corporation (USA), Optech Inc. (Canada) and TopEye AB (Sweden), which comprise the commercial market, covering about 68% of the total market. Remaining 32% is covered by proprietary systems (Flood, 1999). The concept of laser scanning is schematically shown in Figure 6.

Figure 6. ALR concept and EarthData AeroScan LIDAR system (courtesy of EarthData Technologies, a professional provider of LIDAR-based mapping).

On average, the laser ranging device can deliver range information with the accuracy of below 10 to 25 cm. Thus, in order to properly utilize this high quality information, the sensor has to be positioned and oriented with a comparable accuracy. Modern GPS/INS systems meet this requirement rather easily, facilitating direct support to the somewhat demanding mapping applications (Lithopoulos et al., 1996; Skaloud et al., 1996; Abdullah, 1997; Grejner-Brzezinska, 1999). A typical topographic ALR device operates at the wavelength range of 1040-1060 nm, with short pulses ~10 ns and beam divergence of ~1 mrad. The travel times are recorded with an accuracy of ~0.1 ns (~3cm), and subsequently converted to distance information. The scan angle is generally less that 30° and the scanning rate ranges from 2 to 25 kHz. The typical flying height, depending on application, ranges from 20 to 6000 m. For example, the EarthData Technologies AeroScan LIDAR system (Figure 6) has a maximum scan filed of view (FOV) of 75 degrees. At 65 m/s airspeed, the along track spacing is about 8 m, while the cross track spacing is roughly 6 m at the maximum scan rate of 7.5 Hz and a 2500 m AGL (above ground level) flying altitude. The illuminated footprint is 0.6 m. Typical accuracies on the ground are 0.25-0.35 m in cross track, 0.2-0.25 m in along track and 0.15-0.25 m in height error. For more information on laser scanning – processing algorithms and applications, the reader is referred to Axelsson (1999) and Wehr and Lohr (1999).

The ALR data form 3D point clusters or lines, where the elevation has a unique value as a function of the horizontal location, with the point density depending on flying height, surface slope, sampling frequency and the laser's field of view. The fact that laser systems provide 3D coordinates can be considered, on one hand, as their limitation, as virtually no object information is provided. In essence, laser scanning is not capable of any direct pointing to a particular object, and the resulting coordinates refer to the footprints of the laser scan. In many cases, the laser data interpretation can only be performed if the oriented image backdrop of the surveyed area is available. On the other hand, direct availability of surface coordinates allows fast and automated data processing. This is definitely advantageous when compared to photogrammetry, which is still predominantly based on manual or semi-automatic processing. The laser scanning system technology is presently considered fairly mature while the data processing and modeling techniques still require research and further developments.

An additional feature that makes laser systems even more attractive is the fact that they can deliver multiple echoes from one laser pulse, for example first and last, which allows the separation of terrain or man-made objects from vegetation, as a laser beam can penetrate the foliage (see Figure 7). Often, multiple echoes can be produced by the edges of the buildings, which supports detection of the break lines. Moreover, some of the systems can provide not only range measurements, but also intensity (reflectance) information, rendering radiometric information about the surveyed area that is primarily used in classification tasks. Airborne laser scanning systems offer new possibilities to survey areas and objects such as dense city areas, power lines, forests, and DEM (Digital Elevation Model) generation for coastal areas and wetlands, which are difficult to capture or analyze by traditional photogrammetric methods.

4.3. ALR vs. photogrammetric data acquisition/processing

Although airborne laser scanning technology competes to some extent with traditional photogrammetry in certain applications, these two technologies are actually complementary; thus their proper integration might result in more accurate and complete mapping products (Toth and Grejner-Brzezinska, 2000). The primary difference between the two technologies (in the context of elevation data acquisition) is that photogrammetry, providing full area coverage, is based on passive monochromatic imaging sensors, while ALR represents an active, high-power sensor, providing point-wise sampling. Laser systems directly provide 3D coordinates, while in photogrammetry these can be obtained through stereo-image data post-processing. One of the complementary aspects of both data types can be observed by analyzing the average accuracy delivered by photogrammetric and LIDAR systems. For example, the vertical accuracy for the 1:12,000 scale images collected by a large format aerial camera ranges typically from 10 to 30 cm. A topographic LIDAR vertical accuracy for the same altitude (~2000 m) amounts to ~12 cm at nadir and 25 cm at the edges of the scan line (corresponds to 75° field of view (FOV)). The image resolution (and thus the feature measurement accuracy) decreases with altitude, reaching roughly 2 m in vertical accuracy at 20,000 ft altitude, while LIDAR system still offers ~25 cm at nadir and ~45 cm for the edges of the 75° FOV. However, the measurable footprint of the LIDAR spots results in an average elevation value, which is very noticeable around discontinuities. Of course, break lines and the like are problematic for the stereo image-extracted

surface too, but for the non-complex image scenes, their point localization usually shows a much better performance.

As far as man-made objects are concerned, ALR and image-based technologies deliver supplementary information. As already mentioned, contrary to photogrammetric methods, the laser does not capture objects directly, but provides dense set of elevation spots instead (see Figure 7) leading to an excellent representation of the surface—independently from the underlying object contents. Image data allow for feature identification (still, the automatic feature extraction problem is far from being resolved), thus overlaying the two data sets might support the automatic feature measurement process.

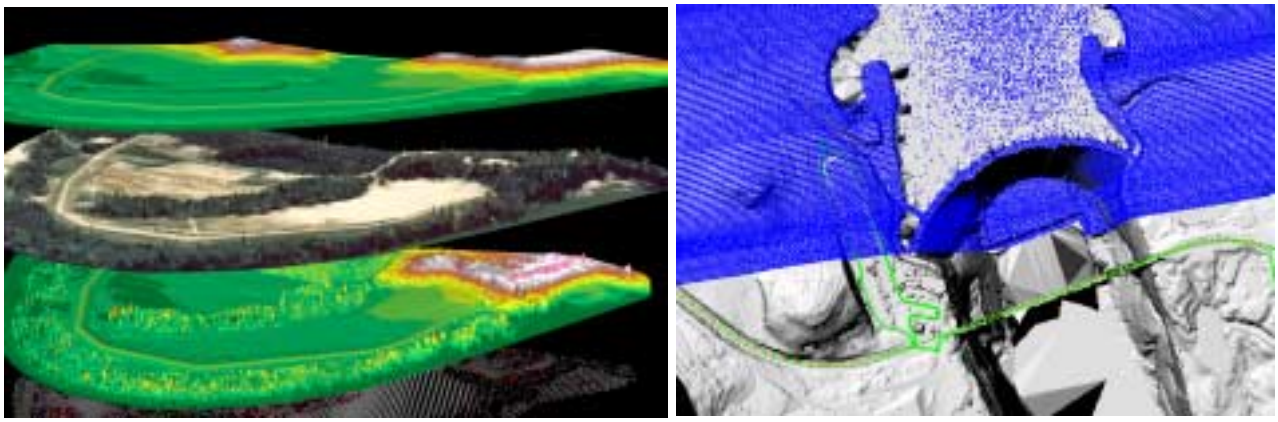

Figure 7. LIDAR surface reconstruction from the first (bottom) and the last returns (left) and LIDAR data (right), (courtesy of EarthData Technologies).

4.4. Multi/hyperspectral sensors

Automation of the map-making process is the ultimate goal of digital photogrammetry, which was the primary driving force behind the MMS technology, that further evolved towards airborne DPO. In general, digital sensors, including multispectral/hyperspectral systems offer the feasibility of automation of the photogrammetric tasks. Since the scope of this report does not allow a full coverage of other modern sensors, such as RADAR and SAR (INSAR), which use DPO as a primary georeferencing tool, as an example a brief description of a hyperspectral sensor is provided below.

Hyperspectral imagery with high spatial resolution opens new remote sensing capabilities, one example being land classification, vegetation, etc. The hyperspectral data contain a large number of narrow spectral channels from the optical wavelength range. The number of channels can vary from several tens to hundreds of channels, with the width of one channel ranging from one to 20 nanometers. Due to the rather complex relationship between the spectral responses of the surface materials, such as vegetation, water, soil, concrete, etc, images of the same object, acquired with a different wavelength, may look quite different. Thus, the hyperspectral systems, by offering numerous spectral bands at each pixel location, provide a wealth of information for classification and image interpretation. In order for this imagery to be useful, however, the geometric

relationship between the pixels on the image and their corresponding locations on the ground has to be known. This task can be accomplished by using the direct platform orientation components to every scan line collected by the hyperspectral sensor.

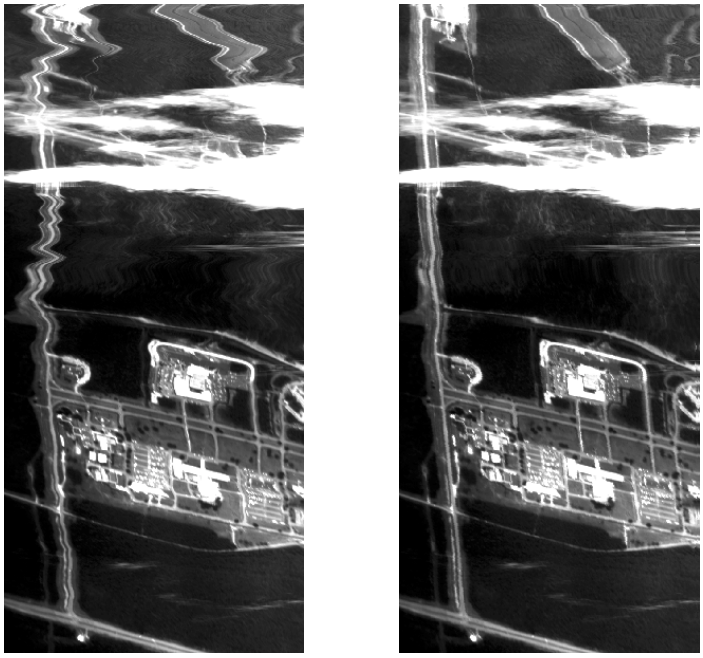

Figure 8. One-channel hyperspectral image (left) and the same image trajectory-rectified (right).

The data collected by a hyperspectral line scanner consist of horizontal imaging scan lines acquired along the aircraft forward motion. An image matrix is directly made from the raw hyperspectral scan lines, showing significant geometric distortions. Primary source of distortions is the air turbulence, which causes the platform instability during the push broom scanning. The left image in Figure 8 represents an original image, consisting of a number of scan lines collected by the hyperspectral sensor. A restored image, corrected by the implementation of the reference trajectory is presented in the right image, displaying a significantly reduced geometric distortions achieved by restoration.

5. WHY DO WE NEED TO INTEGRATE GPS AND INS?

With the increasing use of modern digital sensors (indicated earlier), including CCD-based cameras and multi/hyper-spectral scanners, radiometers, LIDAR, SAR (IFSAR), etc., multi-sensor data fusion has become a crucial step in design of a mobile mapping system (especially airborne), and spatial data processing algorithms. The fundamental step of any data integration process is georeferencing or geometric fusion of data (time-space registration), most commonly provided by GPS/INS. Perhaps it is worthwhile to emphasize here that the use of GPS/INS-derived DPO is mandatory for mapping sensors that work in a continuous scanning mode (multi/hyper-spectral scanners), and for non-conventional (non-optical, such as LIDAR) imaging sensors. However, for analog or digital area-based sensors, direct georeferencing, although not compulsory, still brings obvious economic benefits by largely eliminating the need for the most

complex task of photogrammetry – aerotriangulation (AT), as explained is Section 3. For example, LIDAR or RADAR systems need accurate platform motion data; otherwise, the high-accuracy potential of the range data cannot be realized. These sensors work with rather high data transmission frequencies (10 kHz or higher), and typically, the platform positioning data represent the most important term in the overall error budget. Consequently, high accuracy and reliability of DPO is crucial, therefore the issue of using an optimal navigation sensor suite is of foremost importance.

5.1. Principles of inertial navigation

This section provides a brief explanation of the principles of inertial navigation, and is intended for readers not familiar with this topic. The scope of this paper allows only presenting the basic theory behind inertial navigation, thus, interested reader is referred for more detail information to, for example, (Britting, 1971; Siouris, 1993).

Contrary to other means of navigation, inertial navigation does not rely on observation of landmarks or celestial bodies or measuring radio signals. Instead, it utilizes the inertial properties of sensors mounted aboard a vehicle, and provides self-contained determination of instantaneous position and other parameters of motion of the vehicle, by measuring a specific force, angular velocity, and time. Inertial navigation provides real-time indication of position and velocity of a moving vehicle using IMU sensors (Inertial Measurement Unit) that react on the basis of Newton's laws of motion (equation 1). Two primary types of IMUs are accelerometers, which sense linear acceleration in the inertial frame (i.e., fixed non-rotating frame), and gyroscopes, which sense the inertial rotational motion (angular rates, angular increments or total angular displacements form an initial known orientation relative to inertial space). Since, according to Einstein's principle of equivalence, accelerometers do not sense the presence of gravitational field (but can sense the reaction due to the gravitational forces), external gravity information (from the model) must be provided to obtain navigation information. In principle, INS requires no external information except for initial calibration (initialization and alignment), including externally provided 3D initial position, velocity and attitude. A stationary self-alignment is routinely performed if no external velocity/attitude data are available. The sensor errors, however, grow with time; therefore INS must be recalibrated periodically to maintain reliable navigation quality. In stand-alone mode the INS navigation results are primarily affected by the initial sensor misorientation, accelerometer biases and gyro drifts, causing a time-dependent positioning error.

$$\ddot{\bar{\mathbf{r}}} = \bar{\mathbf{a}} + \bar{\mathbf{g}} \qquad (1)$$

Where $\ddot{\bar{\mathbf{r}}}$ is the total inertial acceleration vector, $\bar{\mathbf{a}}$ is the specific (applied) force vector, $\bar{\mathbf{g}}$ is the total gravitational acceleration vector at the vehicle location.

Gyroscopes are mechanisms displaying strong angular momentum characteristics, capable of maintaining a known spatial direction through an appropriate torque control, since inertially referred rate of angular momentum is proportional to the applied torque. Consequently, the gyroscopes maintain knowledge of the orientation of the inertial platform, upon which orthogonal triad of accelerometers is mounted. Three mutually orthogonal gyroscopes can facilitate a three-dimensional inertially non-rotating Cartesian frame, if mounted on a gimbaled

platform maintaining the gyros orientation in space (space-stable system). However, the platform can be commanded to facilitate other frames of reference, such as most commonly used local navigation frame (local-level system), north-east-down (NED, or n-frame). Alternatively, gyros can be mounted directly on the vehicle (strapped down to the vehicle). In this case, since there is no gimbal platform performing the torque to maintain the gyroscopes' orientation, the torque is applied mathematically directly to the gyros. Since the physically or mathematically applied torque is proportional to the gyro's inertially referenced angular motion, it can be used to calculate the relative angular orientation between the gyro's initial and present spatial direction. The systems with no moving parts (no gimbaled platform), where the instrumentation of a reference frame is not facilitated physically but rather analytically, are referred to as strapdown inertial navigation systems. Since that lack of gimbaled structure allowed for reduction in weight, size, power consumption, and ultimately – cost – they are primary modes of inertial navigation in mobile mapping systems.

The fundamental concept of inertial navigation is that the velocity and position are obtained through real-time integration of the governing differential equations (equations of motion, equation 2), with measured specific force (compensated for earth's gravitational attraction) as an input. As explained above, in inertial navigation, the accelerometers provide the inertial accelerations, and the gyroscopes provide means of controlling the coordinate reference frame, since the frame, in which the vehicle navigates, is different from the inertial frame. In particular, strapdown inertial navigation algorithm facilitates the rotation between the navigation and the INS body frames (b-frame), through the algorithmic compensation (by earth rotation) of the inertial rotations sensed by gyroscopes. General form of the differential equations that describe the motion of a point mass over the surface of the earth is represented by equation (2), while Figure 9 illustrates the basic strapdown mechanization principles.

$$\begin{aligned} \dot{\bar{\mathbf{r}}}(t) &= \bar{\mathbf{v}}(t) \\ \dot{\bar{\mathbf{v}}}(t) &= \bar{\mathbf{a}}(t) + \bar{\mathbf{g}}(\mathbf{r}) - (2\omega_{ie} + \omega_{en}) \times \bar{\mathbf{v}}(t) \end{aligned} \qquad (2)$$

Where :

$\bar{\mathbf{a}}(t)$ – acceleration due to applied force sensed by accelerometer

$\bar{\mathbf{g}}(\mathbf{r})$ – gravitational acceleration

$\mathbf{r}$ – geocentric vector of vehicle position

$\bar{\mathbf{v}}(t)$ – velocity of the vehicle relative to the earth defined in the navigation system

ω_{ie} – earth rotation rate

ω_{en} – angular rate of the navigation frame relative to the earth

Errors in inertial navigation are functions of the following factors: (1) initial condition errors (as a dead reckoning device, INS must know the initial conditions of the position and velocity from the external source, while direction of the initial velocity vector is determined by the process of alignment; a quality strapdown INS system such as LN100 form Litton Guidance and Control Systems, can align itself with high accuracy of 2 arcsec after 4 minutes of standard alignment period), (2) errors in gravitational attraction compensation, (3) errors in coordinate transformation, and (4) time-dependent sensor errors such as accelerometers and gyroscopes,

and possibly external navigation aids used, and finally (5) errors excited by the dynamics of the vehicle. As a consequence, the INS-determined vehicle trajectory will diverge from the actual path, depending primarily on the quality of the IMU sensors and the mission duration. A high-reliability and medium accuracy strapdown INS system, such as LN100 (based on Zero-lock^{TM} Laser Gyro (ZLG^{TM}) and A-4 accelerometer triad, gyro bias – 0.003°/h, accelerometer bias – 25μg) demonstrates the positioning quality of 0.8 nmi/h CEP (circular error probable rate, at 50% probability level) in stand-alone navigation mode. Generally speaking, for the aircraft mission of less than about four hour in duration, the horizontal error growth is statistically characterized by the slope of a straight-line statistical fit CEP to the ensemble of test runs, which typically average about 1.852 km/h (May, 1993). Table 4 below provides representative error characteristics of a medium quality unaided inertial navigator. A comparison of the INS-derived trajectory with the GPS solution is presented in Figure 9.

Table 4. INS performance error characteristics assuming 4-8 min alignment (May, 1993).

Position	0.8 nmi/h (CEP)
Velocity	2.5 ft/s (RMS)
Heading	0.1 deg (RMS)
Pitch and roll	0.05 deg (RMS)
Angular rate	0.04 deg /s (RMS)

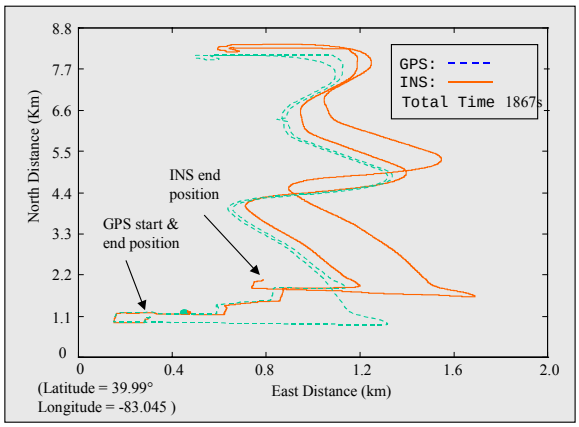

Figure 9. Comparison of GPS and INS stand-alone vehicle trajectories.

5.2. Strapdown inertial navigation

All inertial navigation systems must perform the following functions (Britting, 1971):

- Facilitate a reference frame for vehicle motion
- Measure specific force
- Have knowledge of earth's gravity field
- Perform time integration of the specific force to obtain velocity and position information

Figure 10 illustrates the process of inertial navigation using a strapdown mechanization, which is, as mentioned earlier, the most commonly used in MMS. The notation used in the figure is as follows: a matrix denoted by C_b^n (equation 3) describes transformation from b-frame to n-frame (NED: north, east, down). The meaning of the notation of the other components is similar, for example, ΔV_{ib}^b denotes the velocity rate of the b-frame with respect to i-frame, coordinatized in the b-frame (second subscript). Velocity and angular rates sensed by the IMU sensors are processed by the navigation algorithm, by (1) applying the Earth and vehicle rate compensation to the directly sensed angular rates to convert them to the body—navigation rates $\Delta\Theta_{nb}^b$ (coordinatized in body frame), (2) using the transformed angular rates, to compute the

transformation matrix C_b^n, which is subsequently used to (3) transform the sensed delta velocities to navigation—inertial velocities (still coordinatized in body frame), which are (4) converted to navigation velocities by applying the gravity compensation (based on the gravity model), and (5) are finally integrated to find position an velocity of the platform (see Figure 10). Vehicle's attitude components (heading κ, pitch ϕ and roll ω) are derived from the components of the transformation matrix C_b^n. In summary, the knowledge of initial 3D position, velocity and orientation of the platform (achieved through initialization and alignment processes) along with the knowledge of inertial Earth rotation and parameters of the selected reference ellipsoid, allow the inertial navigator to derive final positioning information in Earth-centered Cartesian frame, and provide NED velocity, as well as heading, pitch and roll.

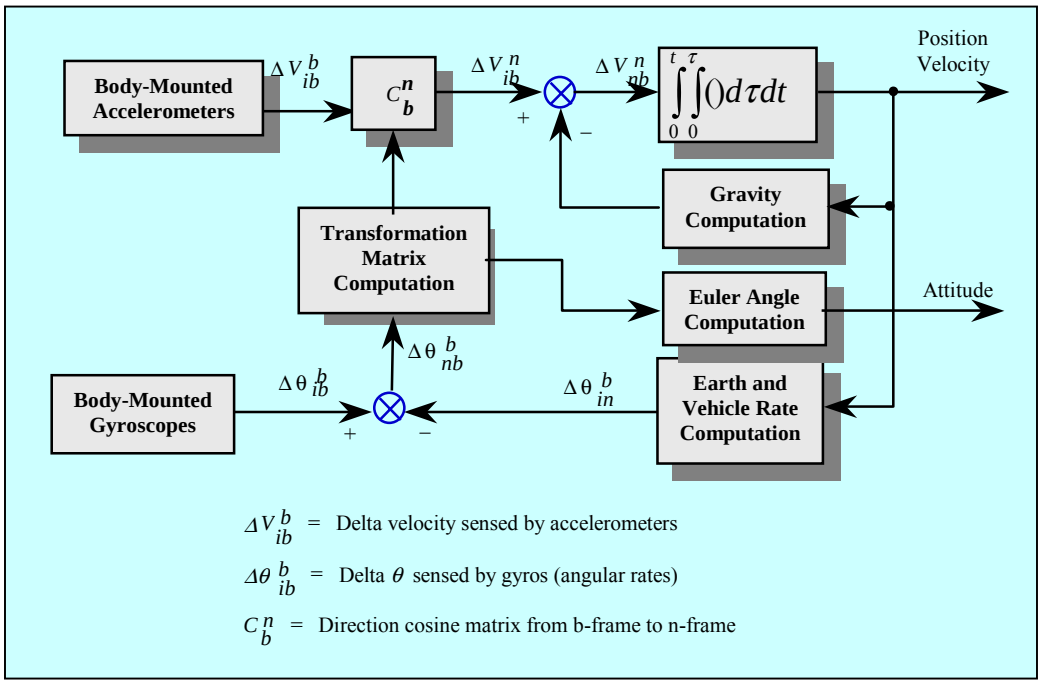

Figure 10. Strapdown inertial mechanization.

$$C_b^n = \begin{bmatrix} \cos\phi\cos\kappa & \sin\omega\sin\phi\cos\kappa - \cos\omega\sin\kappa & \cos\omega\sin\phi\cos\kappa + \sin\omega\sin\kappa \\ \cos\phi\sin\kappa & \sin\omega\sin\phi\sin\kappa + \cos\omega\cos\kappa & \cos\omega\sin\phi\sin\nu - \sin\omega\cos\kappa \\ -\sin\phi & \sin\omega\cos\phi & \cos\omega\cos\phi \end{bmatrix} \quad (3)$$

5.3. GPS/INS integration

GPS and INS, as navigation techniques, offer highly complementary operational characteristics by using entirely different positioning principles – a radio navigation satellite system, GPS provides essentially geometric information (and thus vector $\bar{\mathbf{r}}$ in equation 1 after proper coordinate transformation) while autonomous INS offers inertial information (and thus vector $\bar{\mathbf{a}}$ in equation 1 after gravity compensation), i.e., the reaction to the applied force. In essence, both

systems have different dynamics and spectral characteristics – GPS position errors contain primarily broadband noise, while INS errors are controlled predominantly by the low frequency components. Consequently, their errors are separable and can be independently observed. GPS in a stand-alone mode provides a position fix as long as it is able to maintain lock to a minimum of four satellites. Some systems are still able to provide a solution with less than four satellites, but the accuracy is substantially degraded, especially if partial loss of lock is quite extensive in time. Naturally, one way to improve the GPS gap bridging is to add an autonomous, passive navigation sensor, such as INS. Most of the modern MMS systems rely on high-accuracy differential GPS and quality strapdown INS, while early systems used simpler, and lower quality dead-reckoning systems (wheel counter or odometer, directional and vertical gyros). Obviously, the accuracy obtained strongly depends on the type of sensors used, and ranges from meters (early systems) to centimeters (new generation MMS).

Inertial navigation systems provide self-contained and independent means of three-dimensional positioning and orientation with potentially high short-term accuracy. In addition, compared to conventional GPS output rate, INS provides much higher positioning update rates (up to 256 Hz). However, INS accuracy degrades over time due to uncompensated gyro and accelerometer errors, as explained in Section 5.1. Thus, with full operational GPS capability, it has been recognized that an optimal combination of GPS with inertial navigation brings a number of advantages over stand-alone inertial or GPS navigation. GPS contributes its high accuracy and stability over time, enabling continuous monitoring of inertial sensor errors. Implementation of closed-loop INS error calibration in Kalman filter environment allows continuous, on-the-fly error update (and thus INS calibration,), leading to increased estimation accuracy. The effective error level depends on systematic and random effects on the GPS measurements, as amplified by satellite geometry. Well-calibrated, GPS-supported INS provides precise position and attitude information between the GPS updates and during GPS losses of lock, facilitating immunity to GPS outages, continuous attitude solution, and reduction of the GPS ambiguity search volume/time, after the signal reacquisition. In general, using a GPS-calibrated, high to medium accuracy inertial system, attitude accuracy in the range of 10-30 arcsec can be achieved (Schwarz and Wei, 1994; Abdullah, 1997; Grejner-Brzezinska, 1997; Grejner-Brzezinska and Phuyal, 1998). In summary, any combination of GPS and INS functionality into a single integrated navigation system represents a fusion of dissimilar, complementary data, and should be able to provide a superior performance as opposed to either sensor in a stand-alone mode. In fact, integration of these two systems is often the only way to achieve the following goals (Greenspan, 1996).

- Maintaining of a specified level of navigation during GPS outages
- Providing a complete set of six navigational parameters (3 positional and 3 attitude components) and high rate (higher that available from conventional GPS, i.e., > 20Hz)
- Reduction of random errors in the GPS solution
- Maintenance of a GPS solution under high vehicle dynamics and interference

It should also be mentioned that direct platform orientation could be achieved as well by means of an array of GPS antennas mounted on a mobile platform with known relationship to the reference frame of an imaging sensor. For the most demanding mapping applications, however, the stand-alone multi-antenna GPS is currently not able to provide acceptable attitude solution.

The actual accuracy, depending primarily on the GPS antenna separation and orientation with respect to line-of-sight, and multipath level, can reach 1-2 arcmin for long baselines of 20-30 m (Lachapelle et al, 1994; Ward and Axelrad, 1997) and about 20 arcmin for a 1-meter baseline. Moreover, attitude is available usually at 1-10 Hz rate, which may not be satisfactory for the fast-moving airborne platforms, where frequency of 64-256 Hz is needed.

A summary of GPS and INS characteristics as independent navigation systems, as well as their complementarity is reviewed in Table 4.

Table 4. GPS/INS summary characteristics.

Characteristics	GPS	INS	GPS/INS
Advantages	• High accuracy of position and velocity estimation • Practically time-independent error spectrum • Moderate accuracy (1-2 arcmin) attitude estimation with multiple antennas	• Self contained and independent system • No gaps in data acquisition • Three positioning and three attitude components always available • High data sampling rate (up to 256 Hz)	• Combine all advantages of both systems • Redundant and complementary data (both systems' errors are separately observable) • Navigation through GPS outages • GPS fixes allow INS error estimation
Disadvantages	• Losses of lock causing gaps in positioning • Low data sampling rate (1-10 Hz) • Slow ambiguity resolution time over long baseline and/or in presence of higher ambient noise • Moderate accuracy (1-2 arcmin) attitude estimation with multiple antennas	• Sensor error grow with time causing positioning error divergence	• No significant limitations • Precise time synchronization needed

5.4. GPS/INS Kalman filter design

There are several alternative integration techniques, which can be selected based on the specific application, performance requirements, installation constraints and cost. The last factor is often decisive, as cost of quality INS is still much higher than GPS. However, there has been a substantial INS price drop over the past few years, which in fact allowed more widespread use of inertial navigation in mobile mapping, leading to a significant improvement in performance, automation and modularization. Three primary integration schemes for GPS and INS are so-called

- uncoupled,

- loosely coupled, and
- tightly coupled modes.

In the uncoupled and loosely coupled modes both sensors GPS and INS provide independent positioning/attitude solutions, which are fed to the integration processor to provide a single combined solution. In addition, in the loosely coupled mode the INS error state feedback is implemented, to rectify the INS navigation solution for the next epoch. The most advanced and algorithmically sophisticated is the tightly coupled mode, where both sensors essentially provide raw data – GPS code and carrier phase measurements and inertial accelerations and angular rates – to a single positioning, usually higher order, Kalman filter. Optionally, in the loosely and tightly coupled modes, GPS tracking loop can be supported by the velocity solution from the Kalman filter (integration processor), resulting in better signal lock over much wider vehicle dynamics and radio interference conditions. In general, the uncoupled mode is inferior in performance to the loosely coupled mode, while the tightly coupled integration mode offers an advanced performance with respect to the loosely coupled mode.

The Kalman filtering is the most suitable technique to combine the inertial and GPS measurements, but it requires adequate dynamics, measurement covariance models for the INS and GPS systems. GPS observations are either the phase or pseudorange types in point positioning or differential modes. Differential phase GPS observations are normally used when the high accuracy is required, and the double differences are formed between the single rover and a ground-based reference station. Various forms of INS error models have been developed in (Britting, 1971; Huddle, 1983; Arshal, 1987; Bar-Itzhack and Berman, 1988), however, all these models can be derived using a unified approach, and are considered equivalent (Goshen-Meskin and Bar-Itzhack, 1992). In the example presented here, the following complete terrestrial psi-angle error model is used (Bar-Itzhack and Berman, 1988):

$$\begin{aligned} \delta\dot{\mathbf{v}} &= -(\omega_{ie} + \omega_{in}) \times \delta\mathbf{v} - \delta\psi \times \mathbf{f} + \delta\mathbf{g} + \nabla \\ \delta\dot{\mathbf{r}} &= -\omega_{en} \times \delta\mathbf{r} + \delta\mathbf{v} \\ \delta\dot{\psi} &= -\omega_{in} \times \delta\psi + \varepsilon \end{aligned} \tag{4}$$

Where:
$\delta\boldsymbol{v}, \delta\boldsymbol{r}, \delta\psi$ - the velocity, position, and orientation error vectors, respectively,
∇ - the accelerometer error vector,
ε - the gyro drift error,
$\delta\boldsymbol{g}$ - the gravity anomaly vector,
f - the specific force vector sensed by accelerometer,
ω_{ie} - rotation vector from the Earth-fixed to the inertial frame,
ω_{en} - rotation vector from the navigation to the Earth-fixed frame,
ω_{in} - rotation vector from the navigation to the inertial frame.

A detailed expression of the INS system error model depends on selection of (sensor-dependent) stochastic models describing the gyro and accelerometer measurement errors, as well as gravity anomaly and deflections. Clearly, the filter design object is to achieve the desired modeling accuracy, without unnecessarily increasing the complexity of the models and, thereby, the filter

(Huddle, 1983). The work involves an interactive and lengthy "tuning" process, in which states are added or deleted, dynamic inter-couplings are changed, and white-noise components are altered. In case of the Airborne Integrated Mapping System (AIMS™), used as example here (Da, 1997; Grejner-Brzezinska, 1997; Grejner-Brzezinska et al., 1998) a single Kalman filter, with a nominal number of states equal to 21 is used to process the GPS double-differenced phases, combined with the inertial data (tight coupling mode). The state unknowns are nine navigation components: three errors in position, three in velocity, and three in orientation, three biases and three scale factors for the accelerometers, three gyro drifts, two deflections of the vertical and the gravity anomaly. In addition, GPS ionospheric delay can be estimated for long baselines for every satellite used in the solution, when dual frequency phase data are available. Moreover, three GPS lever arm errors can be included in the filter model in case the GPS antenna and the IMU center offsets are not precisely known. The equation 5 represents a matrix form of the filter state equations.

$$\begin{bmatrix} \dot{\mathbf{x}}_{Nav} \\ \dot{\mathbf{x}}_{Grav} \\ \dot{\mathbf{x}}_{Acc} \\ \dot{\mathbf{x}}_{Gyro} \\ \dot{\mathbf{x}}_{Ant} \\ \dot{\mathbf{x}}_{GPS} \end{bmatrix} = \begin{bmatrix} F_{11} & F_{12} & F_{13} & F_{14} & 0 & 0 \\ 0 & F_{22} & 0 & 0 & 0 & 0 \\ 0 & 0 & 0 & 0 & 0 & 0 \\ 0 & 0 & 0 & 0 & 0 & 0 \\ 0 & 0 & 0 & 0 & 0 & 0 \\ 0 & 0 & 0 & 0 & 0 & 0 \end{bmatrix} \begin{bmatrix} \mathbf{x}_{Nav} \\ \mathbf{x}_{Grav} \\ \mathbf{x}_{Acc} \\ \mathbf{x}_{Gyro} \\ \mathbf{x}_{Ant} \\ \mathbf{x}_{GPS} \end{bmatrix} + \begin{bmatrix} \mathbf{w}_{Nav} \\ \mathbf{w}_{Grav} \\ \mathbf{w}_{Acc} \\ \mathbf{w}_{Gyro} \\ 0 \\ \mathbf{w}_{GPS} \end{bmatrix} \tag{5}$$

where $\mathbf{x}_{Nav}$, $\mathbf{x}_{Acc}$, $\mathbf{x}_{Gyro}$, $\mathbf{x}_{Grav}$, $\mathbf{x}_{Ant}$, and $\mathbf{x}_{GPS}$ are, respectively, the error vectors of the inertial navigation solution, the accelerometer measurement error, the gyro measurement error, the gravity anomaly and deflections, the antenna lever arm errors, and the GPS ionospheric errors (these are estimated for baselines >10 km, when dual frequency phase data are available); $\mathbf{w}_{Nav}$, $\mathbf{w}_{Acc}$, $\mathbf{w}_{Gyro}$, $\mathbf{w}_{Grav}$, and $\mathbf{w}_{GPS}$ are all zero-mean Gaussian white noise vectors. The matrices F_{1j} (j=1,2,3,4) and F_{22} are provided in Appendix A (Da, 1997; Grejner-Brzezinska and Wang, 1998).

6. DIRECT VS INDIRECT SENSOR ORIENTATION

Sensor orientation, also called image georeferencing, is defined by a transformation between the image coordinates specified in the camera frame and the selected mapping reference frame. This process requires knowledge of the camera interior and exterior orientation parameters. The interior orientation (IO), i.e., principal point coordinates, focal length and lens geometric distortion characteristics are only concerned with the modeling of the camera projection system, and are provided by the camera calibration procedure (traditionally, analog cameras are laboratory-calibrated, while digital cameras are calibrated using well-defined indoor or outdoor calibration ranges, see Section 7). On the other hand, the EOP directly define the position and orientation of the camera at the moment of exposure. In traditional airborne surveying, the exterior orientation parameters are obtained by aerial triangulation (AT) based on the object space information (ground control points) and their corresponding image coordinates. As a result of using a mathematical model (collinearity equations) representing the transformation between

the object and image spaces, the EOP are determined, providing a relationship between the image coordinates and the global (or local) mapping reference frame. The combined bundle adjustment usually facilitates not only EOP determination, but may also involve rectification of the camera IO, pre-determined by laboratory calibration procedure. Unfortunately, the significant part of the AT cost is associated with the establishment of ground control points, which might be prohibitive in cases of mapping of remote areas. Consequently, the direct orientation provided by GPS/INS (i.e., direct EOP or DOP, without a process of AT), is highly advantageous (provided that the satisfactory accuracy level is achieved), as it virtually eliminates most of ground control, and problems of image matching and need of approximate tie points required for automatic AT to recover exterior orientation (EO). However, a crucial point of application of direct georeferencing is the accuracy and reliability of DPO, depending primarily on sensor quality, stability and accuracy of the system calibration, quality of time synchronization, and the type of the data processing algorithm.

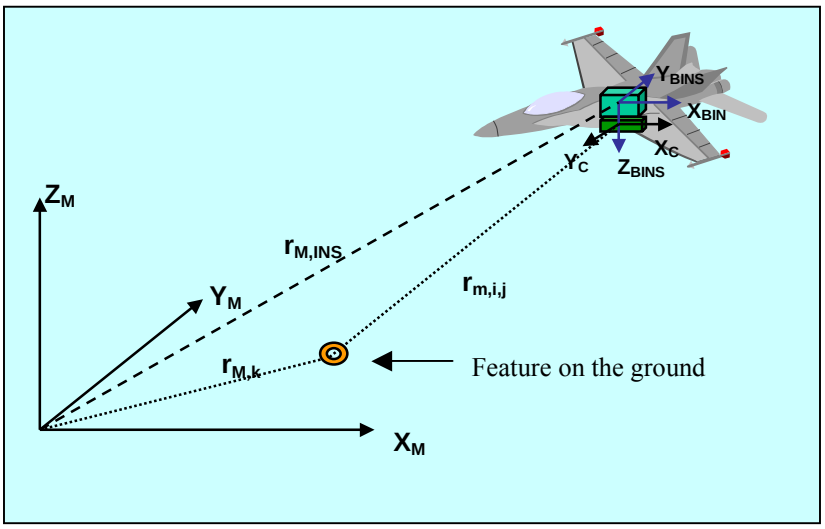

Figure 11. Direct georeferencing: the concept.

DPO, as explained earlier, can be accomplished by inertial navigation or a multi-antenna GPS, or, for the highest accuracy, by integration of both systems to utilize their complementary features (see Section 5.3). Thus, based on discrete measurements, georeferencing determines the time-dependent vector $r_{M,INS}(t)$ and matrix $R^{M}_{BINS}(t)$ (see equation 7), hence the problem is equivalent to finding six parameters of rigid body motion, under the assumption that the sensor is a rigid body. Since we are dealing with discrete observations, some modeling and estimation are introduced to relate measurements to the unknown filter states, and interpolation is needed to relate the estimated trajectory to the epochs of image exposure. In principle, no external information such as ground control is needed, except for the GPS base station and the boresight calibration range, which is usually needed prior to the mapping mission.

Since the DPO rotational components are naturally related to the INS body frame, in order to relate the GPS/INS-derived positions, INS-derived attitude components and image point coordinates, a multi-sensor system calibration is required (see Section 7). This procedure must be able to resolve (with a sufficient accuracy) the misalignments between the INS body frame and

the imaging sensor frame (boresight transformation), and GPS/INS lever arm. The boresight components are usually determined on a specialized test range, while the linear offsets between the GPS antenna phase center and the center of the INS body frame are precisely measured using traditional surveying techniques. In addition, an imaging sensor must be calibrated to determine the camera interior orientation. The concept of georeferencing is illustrated in Figure 11 and described in a form of the coordinate transformation in equation 2, while the operational architecture of DPO determination with GPS/INS is presented in Figure 12.

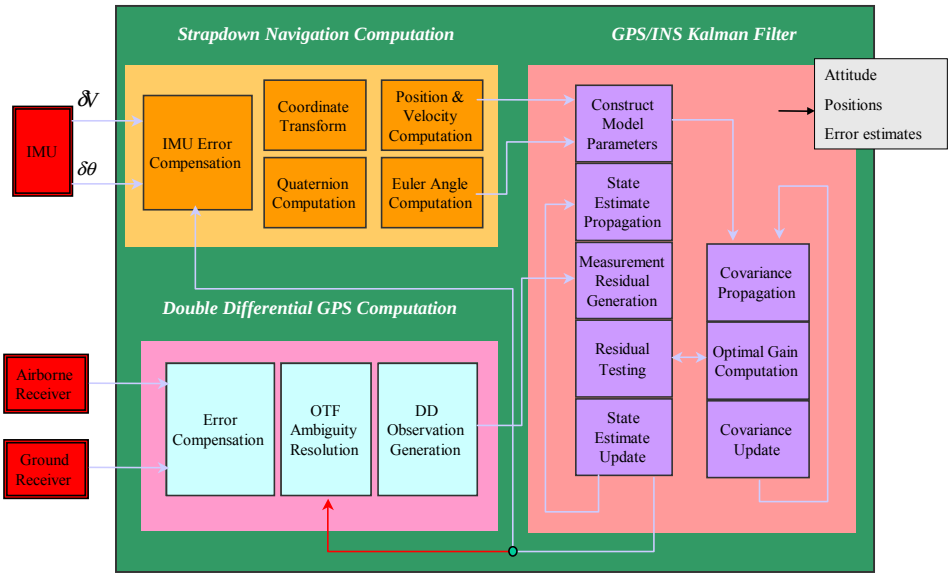

Figure 12. Operational architecture of DPO determination with GPS/INS.

The mapping frame (m-frame) introduced in Figure 11 and equation 7 can be any 3D geodetic reference frame, such as WGS84, NAD83 or UTM (plus the height information) or any other selected Earth-fixed reference system. The body frame (b-frame) is defined as the INS sensor frame, attached to the IMU chassis. If the sensors are rigidly mounted in the vehicle (i.e., aircraft), the changes of b-frame with respect to m-frame follow the motion of the aircraft. For the m-frame selected as a local level frame, East-North-Up (ENU), the three rotations by heading, pitch and roll angles, defined as $R_{\omega\phi\kappa}$, provide transformation from b to m-frame (equivalent to $R^{M}_{BINS}(t)$ in equation 7, where time argument indicates that this matrix varies with the motion of the platform). If the m-frame is selected as a 3D Earth-centered-fixed Cartesian frame (ECEF), the matrix $R^{M}_{BINS}(t)$ becomes a product of $R_{\omega\phi\kappa}$ (provided by INS) and R^{ECEF}_{ENU} (see equation 6); the subscript t indicates the time-dependence as a function of the platform coordinates, latitude φ and longitude λ.

$$R^{M}_{BINS}(t) = R^{ECEF}_{ENU}(t) \cdot R_{\omega\phi\kappa}(t) = \begin{bmatrix} -\sin\lambda & -\sin\varphi\cos\lambda & \cos\varphi\cos\lambda \\ \cos\lambda & -\sin\varphi\sin\lambda & \cos\varphi\sin\lambda \\ 0 & \cos\varphi & \sin\varphi \end{bmatrix}_t \cdot R_{\omega\phi\kappa}(t) \qquad (6)$$

$$r_{M,i} = r_{M,INS}(t) + R^{M}_{BINS}(t)\left(s \cdot R^{BINS}_{C} \cdot r_{C,j} + b_{BINS}\right) \qquad (7)$$

where :

$r_{M,i}$ – *3D object coordinates in mapping frame*

$r_{M,INS}(t)$ – *time dependent 3D INS coordinates in mapping frame, provided by GPS/INS* (*refers to the origin of INS body frame*)

$r_{C,j}$ – *image coordinates of the object in camera frame C*

R_C^{BINS} – *boresight matrix between INS body and camera frame C*

$R_{BINS}^M(t)$ – *time dependent rotation matrix between body and mapping frames* (*measured by INS*)

s – *scaling factor*

b_{BINS} – *boresight offset vector*

6.1. Some limiting factors

Since contrary to a traditional bundle adjustment, in DPO applications, the IO and EOP estimation processes are decoupled (no common adjustment procedure that could compensate for imprecise IO or boresight transformation parameters), it is crucial that the calibration parameters (both IO and boresight) are estimated with high level of accuracy and reliability, and stay constant for the entire mission duration. Another crucial factor for reliable DPO is the precise time synchronization (as explained in Section 2) usually realized by the exchange of synchronization signals, which relate different sensors to a common time frame provided by GPS. The quality and stability of calibration and time synchronization are especially important for airborne systems, where the object distance is significantly larger as compared to the land-based applications. Any error in IO, timing or boresight components would translate directly into errors in ground coordinates of the extracted objects. For example, the time alignment must be good to at least 0.1msec, if one wants to avoid cm-level and larger errors due to lack of synchronization; 0.1msec translates to 0.6 cm positioning error, assuming 60 m/s aircraft speed. To summarize, the overall performance of the direct orientation method is limited primarily by the following components (as explained in more details in the following sections):

- Quality of the calibration of the integrated system:
  - Imaging sensor modeling
    - Interior orientation
    - Camera geometry and resolution
    - Image capture rate
  - Lever arm between INS and GPS antenna
  - Boresight transformation between INS and camera frames
- In-flight variation of the individual sensor calibration components
- Rigidity of the common mount of the imaging sensor and INS
- Quality of the IMU sensor
- Continuity of the GPS lock
- GPS/INS Kalman filter design and implementation
- Feature extraction method – affects the overall accuracy of the final mapping product

To illustrate the effect of the quality in DPO on the positioning accuracy of the ground points extracted from the directly oriented airborne imagery, Table 5 presents the results of the simulations where a representative sample of 2000 sets of von Gruber points (six evenly distributed points in an image) was generated for every set of assumed errors in attitude and projection center location, and the resulting mean error, median and RMS for the ground point location were computed. Focal length of 0.05 m and flight altitude of 300 m were assumed, which represents a typical scenario of the low-altitude mission with a medium format digital frame camera. It can be observed from the table that for the fixed error in the exposure center coordinates, the increase in the attitude error (to the extent considered here) does not significantly change the ground position error. Consequently, an increasing error in the exposure center coordinates shows increase in ground coordinate errors comparable for all the levels of errors in attitude analyzed here. This can be explained by the fact that the assumed errors in attitude are relatively small, compared to the assumed errors in exposure center coordinates, and their projection to the ground level from 300 m amounts to about 7 mm for 5 arcsec error, 1.4 cm for 10 arcsec, 3 cm for 20 arcsec, 4.3 cm for 30 arcsec, and 8.7 cm for 60 arcsec. They become more important for higher altitude flights and in situations where the exposure centers are estimated with high accuracy (below 10 cm), which is currently achievable with quality GPS/INS systems.

The crucial factors limiting the DPO quality are the accuracy and stability of multi-sensor system calibration and the camera IO. Accurate and invariable boresight transformation, precise time synchronization and precise estimation of the IO parameters are the most important calibration components, impacting the overall accuracy of DPO and the object space coordinates. Any error in IO will directly affect the ground coordinates, as DPO provides no compensation for erroneous or imprecise IO, as opposed to a bundle adjustment. From this stand point, the integration of GPS/INS into a combined AT might provide the best and most reliable solution, as camera calibration (self-calibration) could be a part of the combined adjustment. Since GPS/INS provide high quality positioning information, the AT process, in principle, would require much less tie points as opposed to AT with no GPS/INS, to correct IO and exterior orientation. Moreover, such a combined procedure would allow for independent boresight estimation based on the image data collected during the actual survey (see, for example Cramer et al., 1999). These issues are more relevant to airborne systems, where the object distance is larger than that of the land-based system, where GPS/INS with carefully calibrated camera and boresight/lever arm is capable of providing high accuracy and reliable DPO (on one hand it is more controllable environment, on the other hand, more GPS losses of lock can occur as opposed to airborne scenario). Nevertheless, the testing against the ground truth should be performed occasionally also for the land-based systems, to assure that no change in calibration components/system configuration, which would impact the DPO estimates, occurred.

Table 5. 3D ground positioning error resulting from the errors in exterior orientation (50-mm and 300-m altitude): simulation results.

Errors in Xo,Yo,Zo $\omega_o,\varphi_o,\kappa_o$	Ground positioning error characteristics		
	Mean [m]	RMS [m]	Median [m]
5 cm, 5”	0.142	0.088	0.119
5 cm, 10”	0.147	0.091	0.128
5 cm, 20”	0.168	0.106	0.142
5 cm, 30”	0.192	0.119	0.163
5 cm, 60”	0.303	0.193	0.254
10 cm, 10”	0.287	0.182	0.239
10 cm, 20”	0.297	0.190	0.248
10 cm, 30”	0.307	0.194	0.260
10 cm, 60”	0.396	0.245	0.346
20 cm, 10”	0.569	0.345	0.488
20 cm, 20”	0.576	0.362	0.488
20 cm, 30”	0.587	0.364	0.502
20 cm, 60”	0.603	0.382	0.504
30 cm, 20”	0. 833	0.528	0.700
30 cm, 30”	0. 858	0.533	0.737
30 cm, 60”	0.879	0.547	0.740

7. MULTISENSOR SYSTEM CALIBRATION

As indicated earlier, a multi-sensor system calibration is an important factor, which directly impacts the overall quality of the DPO parameters, and ultimately the mapping job. System calibration is defined here as determination of spatial and rotational offsets between the sensors (GPS/INS lever arm and INS/camera boresight components), as well as imaging sensor calibration, since for DPO application the stability and accuracy of the interior orientation parameters of the imaging sensor is mandatory. The calibration parameters must be determined with the highest achievable accuracy and must remain constant for subsequent mapping missions. In other words, no flex or rotation can occur between the INS and camera devices; the common mount should be sufficiently rigid. Multisensor calibration is discussed in details in (Grejner-Brzezinska, 1999), but for the sake of completeness, it is also presented here, with some references to the results described in (ibid.).

7.1. Camera calibration

In most general terms, calibration can be defined as a refined form of measurement performed to assign numbers that represent relationships among particular properties of a measurement system. Geometric camera calibration is a fundamental prerequisite for any vision system that relies on quantitative measurements of the observed scene. The camera calibration is a process of determining the internal geometric and optical characteristics (intrinsic parameters, or camera interior orientation represented by focal length, location of the principal point, and coefficients of appropriate models representing lens distortion), and the 3D position and orientation of the camera frame relative to a certain world coordinate system (extrinsic parameters, or spatial

relationships of the imaging system). For the camera calibration purposes the classical photogrammetric collinearity equations are extended to include the interior orientation, thus the adjustment procedure produces the calibration results and the 3D coordinates of the object targets, as well as exterior orientation. However, due to correlation among the unknown parameters, the geometry of the calibration network must be very strong. This requires a 3D set of large number of points, and wide range of camera orientations at the exposure times. If the measurement system includes additional sensors, their relative spatial position and orientation properties must also be determined by calibration. The calibration procedure should include environmental influences if the full capability of the spatial accuracy of the system is to be realized. Naturally, the level of accuracy required by the calibration procedure depends on the specifications of the measurement system determined by the camera type, by other components of the measurement system, and by the projected accuracy to be delivered by the calibrated measurement system. Proper calibration of the camera and its associated system components is mandatory for any reliable system performance analysis or prediction.

Traditionally, photogrammetric cameras have been periodically laboratory-calibrated. Since CCD-based cameras are not professional metric devices, their calibration raises some issues, such as the long-term stability of the parameters and the way, in which the calibration should be or can be performed (for example, collimators built for calibrating large format aerial cameras cannot properly handle the small sensor size). This naturally leads to self-calibration techniques and to the use of various test fields, including in-flight scenarios. Self-calibration techniques are well understood and widely used, and literature exists on this topic (see for example, Robson et al. 1998). As an example, the calibration results of the BigShot™ 4K×4K CCD with Carl Zeiss Distagon 4/50-mm lens are presented below. For the calibration purpose, the image coordinate pairs of ~300 points evenly distributed in 3D indoor test range were measured on images acquired from different exposure stations, and subsequently processed with the OSU CEEGS Bundle-Adjustment with Self-Calibration (BSC) software, providing estimates of IO. The additional parameters for decentering distortion and the affine transformation for scale differences between axes were constrained to zero for compatibility with the SoftPlotter distortion model. The calibration was repeated independently three times, including also the outdoor test range, and the results are presented in Table 6.

Table 6. 4K by 4K BigShot™ camera equipped with 50-mm lens: calibration parameters.

Parameter	Calibration 1		Calibration 2		Calibration 3		Calibration 4	
	Value	Sigma	Value	Sigma	Value	Sigma	Value	Sigma
C (mm)	51.568	0.008	51.762	0.008	51.688	0.008	51.570	0.007
Xp (mm)	0.314	0.010	0.669	0.005	-0.075	0.004	0.296	0.004
Yp (mm)	0.112	0.013	0.227	0.005	0.376	0.005	0.073	0.005
Rad1 (K1)	-2.77E-05	9.35E-07	-2.71E-05	3.40E-07	-2.76E-05	2.80E-07	-2.68E-05	4.14E-07
Rad2 (K2)	1.44E-08	5.77E-10	1.38E-08	2.50E-10	1.36E-08	9.30E-09	1.35E-08	3.07E-10

The results of four independent calibrations indicate that while the distortion model and focal length do not change significantly, the major variation can be observed in the principle point location. This is a natural consequence of the fact that the camera presented here is not a rigid device (this does not apply, however, to all digital cameras); the camera body and the camera

back housing the CCD chip are rather loosely connected, thus any time the camera back is removed and re-attached to the camera body, significant change in the principle point location should be expected, and calibration should be performed. Consequently, the self-calibration during the actual project is advisable, if an adequate test field is available, as it brings the advantage of calibrating under the same conditions as the factual image collection.

7.2. Boresight transformation

The use of directly measured EO parameters requires knowledge of the transformation between GPS/INS and camera frames, known as boresight transformation. The two components of boresighting are the offset vector between the INS center and the camera perspective center, and the rotation matrix from the INS body frame to the camera optical axis (see equation 7 and Figure 11). The critical component is the rotational offset, since the angular inaccuracy, unlike a linear offset, is amplified by the object distance and has a significant impact on the photogrammetric data production, especially in airborne scenario (see example below and Table 8). The boresight transformation is most commonly resolved by comparing the GPS/INS positioning/orientation results with an independent AT solution (see an example below), or as a part of a bundle adjustment with constraints (see for example El-Sheimy et al. 1995; Cramer et al., 1999). Thus, the quality of the boresight estimation is limited by the quality of the AT adjustment and the quality of the direct orientation components that are used in the boresight estimation process. Consequently, the availability of a high quality test range with very well signalized points that should be used for the calibration process becomes an important issue. Our practical experiences, especially in airborne tests, indicate that even if the control points are surveyed with cm-level accuracy on the ground, their poor signalization (non-symmetric marks, natural targets) may propagate to the projection centers' positioning quality (in the AT process), immediately compromising the boresight performance (see Section 8.2).

The boresight calibration, when resolved by comparing the GPS/INS results with an independent AT solution on a test range, can be accomplished in two steps: first, computation of the displacement between the center of the INS body frame and the camera projection center; second, determination of the boresight matrix. The following simple mathematical model can be used in step one:

$$\overline{X}_{NED}^{INS} = \begin{bmatrix} X_{INS} \\ Y_{INS} \\ Z_{INS} \end{bmatrix}_{NED} = \begin{bmatrix} X_{PC} \\ Y_{PC} \\ Z_{PC} \end{bmatrix}_{NED} + R_{BINS}^{NED} \cdot \begin{bmatrix} b_x \\ b_y \\ b_z \end{bmatrix} = \overline{X}_{NED}^{PC} + R_{BINS}^{NED} \cdot b_{INS} \qquad (8)$$

Where b_x, b_y, b_z are the boresight offsets defined in the INS body frame, R_{BINS}^{NED} is the attitude matrix obtained by INS, and vectors $\overline{X}_{NED}^{INS}$ and $\overline{X}_{NED}^{PC}$ denote INS body center and camera projection center at given epoch, respectively, defined in NED (North-East-Down) local Cartesian frame. Both vectors are known either from the GPS/INS ($\overline{X}_{NED}^{INS}$) or the AT ($\overline{X}_{NED}^{PC}$) solutions, and the R_{BINS}^{NED} matrix is measured by INS, thus the only unknown in equation 8 is vector b_{INS}.

In order to determine the boresight rotation angles, the reflection matrix *S* is applied first to the INS-derived attitude matrix to obtain a rotation matrix R_{BINS}^{ENU} related to the axes defined according to the photogrammetric principles (INS/GPS local reference frame is defined as NED, whereas the photogrammetric system is defined by ENU (East-North-Up), as shown in equation 9, where:

$$R_{BINS}^{ENU} = S \cdot R_{BINS}^{NED} \tag{9}$$

$$S = \begin{bmatrix} 0 & 1 & 0 \\ 1 & 0 & 0 \\ 0 & 0 & -1 \end{bmatrix} \tag{10}$$

The difference between the matrix R_{BINS}^{ENU} and the photogrammetrically derived attitude matrix R_{Pht}, defines the angular misalignments between both systems. The following mathematical model (11) describes the computation of boresight matrix R_C^{BINS}. The final boresight rotation angles, δheading (δκ), δpitch (δϕ), and δroll (δω) are extracted according to equations 12. It should be mentioned here that if multiple stereo pairs with control point are provided, the algorithm presented here can be implemented as least squares adjustment to achieve higher accuracy of the boresight components.

$$R_{Pht} = R_C^{ENU} = R_{BINS}^{ENU} \cdot R_C^{BINS} \Rightarrow \quad R_C^{BINS} = R^{T}{}_{BINS}^{ENU} \cdot R_C^{ENU} \tag{11}$$

$$\begin{aligned} \delta\phi &= \sin^{-1}(r_{13}) \\ \delta\omega &= \tan^{-1}\left(\frac{-r_{23}}{r_{33}}\right) \\ \delta\kappa &= \tan^{-1}\left(\frac{-r_{12}}{r_{11}}\right) \end{aligned} \tag{12}$$

where

$$\begin{bmatrix} r_{11} & r_{12} & r_{13} \\ & r_{22} & r_{23} \\ & & r_{33} \end{bmatrix} = R_3 R_2 R_1 = R_\kappa R_\phi R_\omega = R_{\omega\phi\kappa} =$$

$$\begin{bmatrix} \cos\delta\phi\cos\delta\kappa & -\cos\delta\phi\sin\delta\kappa & \sin\delta\phi \\ \cos\delta\omega\sin\delta\kappa + \sin\delta\omega\sin\delta\phi\cos\delta\kappa & \cos\delta\omega\cos\delta\kappa - \sin\delta\omega\sin\delta\phi\sin\delta\kappa & -\sin\delta\omega\cos\delta\phi \\ \sin\delta\omega\sin\delta\kappa - \cos\delta\omega\sin\delta\phi\cos\delta\kappa & \sin\delta\omega\cos\delta\kappa + \cos\delta\omega\sin\delta\phi\sin\delta\kappa & \cos\delta\omega\cos\delta\phi \end{bmatrix}$$

Example

The estimation of the boresight transformation for a land-based MMS was performed based on the algorithm presented above. The object distance ranged from ~10 to ~12 m, and a specialized test range was used, thus, the AT performance was very good, as presented in Table 7. Since the

GPS/INS also provided quality solution (1-2 cm for positions and ~10 arcsec for attitude), the resulting boresight parameters were of good quality, with RMS of 2-3 cm for offsets, 15-20 arc sec for angular components (which, based on Table 8, should introduce positioning error no bigger than 2 cm even for very long object distance; see explanation below). Another example of boresight estimation based on the natural targets (as opposed to a specialized range) is presented in Section 8.2.

Table 7. AT performance on the boresight range.

Point ID	E [m]	N [m]	H [m]	E residual [m]	N residual [m]	H residual [m]
14	553789.008	221908.411	212.473	-0.003	-0.001	0.002
15	553789.426	221909.427	212.448	-0.006	0.002	0.000
24	553788.985	221908.418	211.366	0.010	0.000	-0.002
25	553789.407	221909.438	211.356	0.009	-0.002	-0.001
34	553788.974	221908.415	210.272	-0.006	0.002	0.001
35	553789.390	221909.437	210.248	-0.004	0.000	0.000
RMS				0.007		0.001

The effects of the boresight quality on the ground object coordinates in the mapping frame can be shown based on the analysis of equation 7, which is the well-known georeferencing formula. Under the simplified assumptions that all the components, except for the boresight misalignments, are error-free and uncorrelated, the covariance matrix of the object ground coordinates can be obtained by the error propagation formula (details are provided in Grejner-Brzezinska, 1999). Table 8 illustrates an example of the effects of the errors in the boresight components on the object ground coordinates. The average location within a 60 by 60 mm imaging area was selected, with a focal length of 50 mm, and object distance of 20 m (land-based applications) and 300 m (airborne applications), respectively; the latitude and longitude were chosen as 40 deg and –81 deg, heading, pitch and roll were selected at 100 deg, 3 deg and 3 deg, respectively for this example.

Table 8. Error in object's ground coordinate in [m] due to boresight errors; 20-meter and 300-meter object distance, and focal length of 50 mm were assumed (Grejner-Brzezinska, 1999).

Error in boresight offset [m]		Error in boresight angles [arcsec]					
		20-m object distance			300-m object distance		
		5	10	20	10	20	60
X	0.02	0.02	0.02	0.02	0.02	0.02	0.03
Y	0.02	0.02	0.02	0.02	0.02	0.02	0.05
Z	0.02	0.02	0.02	0.02	0.02	0.02	0.04
X	0.05	0.05	0.05	0.05	0.05	0.05	0.06
Y	0.05	0.05	0.05	0.05	0.05	0.06	0.10
Z	0.05	0.05	0.05	0.05	0.05	0.06	0.10
X	0.10	0.10	0.10	0.10	0.10	0.10	0.11
Y	0.10	0.10	0.10	0.10	0.10	0.10	0.14
Z	0.10	0.10	0.10	0.10	0.10	0.11	0.13

7.3. Lever arm calibration

The three lever arm components are the linear offsets between the INS body center and the GPS antenna phase center, defined in the INS body frame. These offsets are usually surveyed very precisely using optical/electronic surveying equipment, and must be known with a sufficient accuracy to guarantee proper transformation of the GPS positions referred to the antenna phase center to (from) the INS body center. Consequently, correctly (incorrectly) defined lever arm have a direct impact on the navigation process and the ambiguity resolution/cycle slip fixing supported by INS. The errors in the lever arm components are constant biases (results of the errors in the original survey) and time-dependent terms (drift in the heading, pitch and roll that occurs during the survey, as attitude angles are used to rotate the nominal offsets during the GPS update epoch, to reduce the GPS positions to the INS center). It should also be mentioned that precise knowledge of the lever arm offsets is especially crucial to the embedded GPS/INS systems, where the INS directly aids the carrier phase tracking loops. The effect of lever arm on the positioning results is illustrated in Figure 13 in terms of the level of double difference phase residuals in case when lever arm is measured incorrectly (left) and with the precise lever arm components.

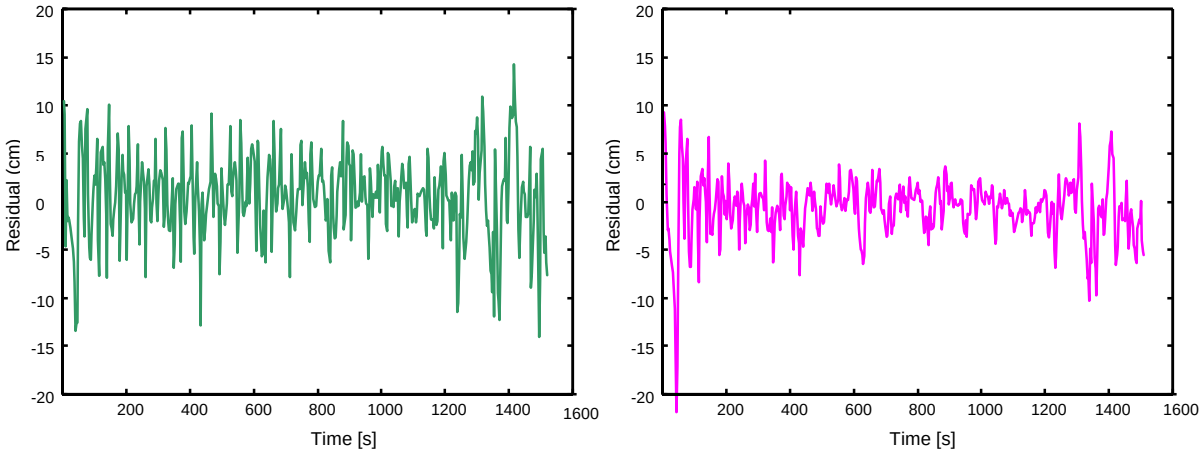

Figure 13. DD Carrier Phase Residuals: level arm errors not calibrated (left) and calibrated (right).

8. CURRENTLY ACHIEVABLE ACCURACY

The early MMS were based on simpler and less expensive than strapdown INS dead reckoning sensors (DR, wheel counters and odometers, vertical and directional gyros), so their final feature positioning accuracy (combined with photogrammetric processing), was estimated at a foot-level (reaching about 10-20 cm level at 5-20 m object distance in mid-1990s; see for example, He et al., 1994; Toth, 1995b), and was lower than the one currently attainable by modern GPS/INS modules (under favorable GPS conditions). Naturally, an effective accuracy is a function of the type of INS sensor used, geometry, quality, continuity and processing mode of GPS data, quality of system calibration, design of the processing algorithm and several other items listed in Section 6.1. Object distance is also an important factor, as the same attitude or boresight errors result in different levels of feature errors, as shown in Tables 5 and 8. One way of testing the quality of

DPO is to use ground control points to perform large-scale photogrammetry (AT) to provide accurate coordinates of the perspective center at the times of exposure, and compare with the DPO results. Another way is to use a consistency check based on multiple GPS station solutions or repeatability conditions. This is an indirect way of QC, but certainly far less expensive than AT. An ultimate quality control is to use known ground control points that can be identified in the imagery, and compare the DOP-supported coordinates of these points with their pre-survey coordinates.

Some examples of the performance assessment of the land-based GPS/DR, and the land-based and airborne integrated GPS/INS system, developed at the Center for Mapping the Ohio State University are presented below. We start with a lower-end system (by today's standards) developed in mid-1990s, and follow with an advanced GPS/INS system used in land-based and airborne applications.

4.1. Accuracy of a land-based MMS with differential GPS and dead reckoning system

An example presented here illustrates a practically achievable accuracy of MMS, GPSVan™, based on differential GPS and independent (loosely-integrated) dead-reckoning system (thus, 1st generation of direct georeferencing sensors), and two digital cameras (768 by 480 pixels resulting in about 1-2 cm nadir pixel size at 10-m object distance) (He et al., 1994; Bossler and Toth, 1995). The performance assessment presented here is based on feature mapping of 7,000 miles of railroad track of the Burlington Northern Santa Fe Corporation (BNSF) (Bossler and Toth, 1995; Grejner-Brzezinska, 1996). On average, the trajectory of the vehicle was estimated at 10 cm level, when GPS data were available at 3-second intervals (GPS data outages of 30, 60, and 120 s cause the positioning degradation to the level of 0.2, 0.4, and 1.0 m, respectively). The achievable quality of GPS is a function of base-rover separation (here, max. 35 miles), satellite geometry and the number and extent of losses of lock. A statistics of GPS accuracy are presented in Figures 14 and 15, which indicate that only 0.1-0.3% of surveys displayed GPS error of 1 m and above, due to (primarily) GPS losses of lock.

Since every survey was performed with dual GPS base stations, the rover trajectories could be computed independently with the two base stations. The difference between both trajectories, as shown in Figure 16, gives further insight into the quality of GPS positioning. The low RMS clearly indicates a consistent GPS processing performance. This positioning accuracy, combined with photogrammetric image processing result in the final accuracy of the mapped features, which is summarized in Figure 17, showing the overall fit to the ground truth. An average planimetric accuracy of about 50 cm (primarily due to the errors in attitude data derived from DR system) for over 95% of the independent checkpoints was demonstrated. It should be mentioned that using higher resolution CCD leads to increased feature positioning accuracy, with the same positioning component used. For example, using a 1K by 1K CCD sensor with 1.8 m camera base results in positioning accuracies that are better than 3 cm for object distances of 5 m and 15 cm for 25 m, respectively.

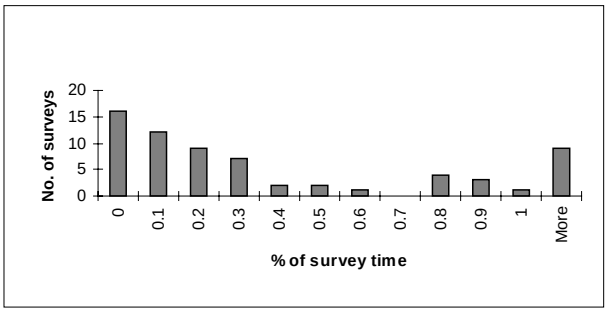

Figure 14. Loss of lock events.

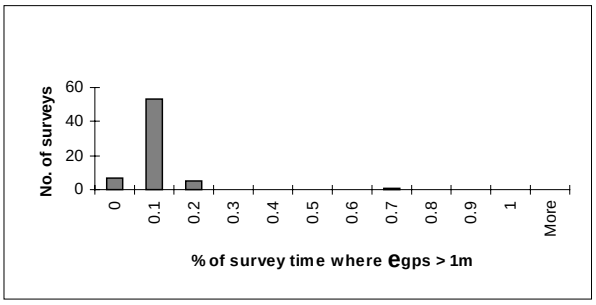

Figure 15. Quality of the GPS positioning (e_{GPS} is a total error in GPS).

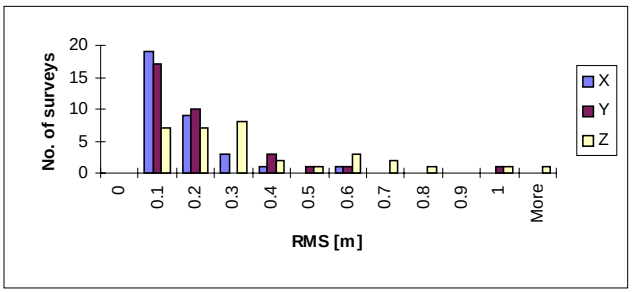

Figure 16. Difference between the two rover trajectories.

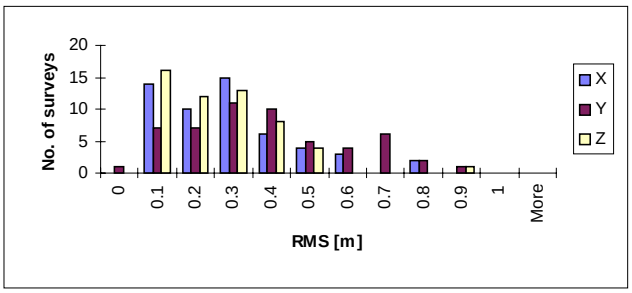

Figure 17. Distribution of differences at QC points.

Naturally, using better DR system, such as for example LN-100 inertial navigation system from Litton Guidance and Control, Inc., based on Zero-lock™ Laser Gyro (ZLG™) and A-4 accelerometer triad will provide much higher positioning accuracy, and will allow using such navigation module in airborne photogrammetry, as presented in the next section. El-Sheimy and Schwarz (1999) report horizontal and vertical accuracies on ground check points within 10-30 m object distance of 0.13 m and 0.08 m (RMS), respectively, achieved with GPS/INS navigation, and RMS of 0.29 m and 0.19 m, respectively, for the free navigation INS mode (GPS outages).

8.2. Accuracy of a land-based and airborne MMS with differential GPS/INS system

As an example, a prototype of the integrated GPS/INS/CCD system, supporting both land-based and airborne mapping, is presented in this section. The imaging component prototype consists of a single digital camera based on a 4,096 by 4,096 CCD with 60 by 60 mm imaging area (15 micron pixel size), manufactured by Lockheed Martin Fairchild Semiconductors, integrated into a camera-back (BigShot™) of a regular Hasselblad 553 ELX camera body. Two Trimble 4000SSI GPS receivers, and a medium-accuracy and high-reliability strapdown Litton LN-100 inertial navigation system (0.8 nmi/h CEP, gyro bias – 0.003°/h, accelerometer bias – 25μg) complete the navigation module. The LN100 firmware version used in this system allows for an access to the raw IMU data, with the update rate up to 256 Hz. Estimation of errors in position, velocity, and attitude, as well as errors in inertial and GPS measurements, is accomplished by a 21-state centralized Kalman filter that processes GPS L1/L2 phase observable in double-differenced mode together with the INS strapdown navigation solution (see Section 5.4).

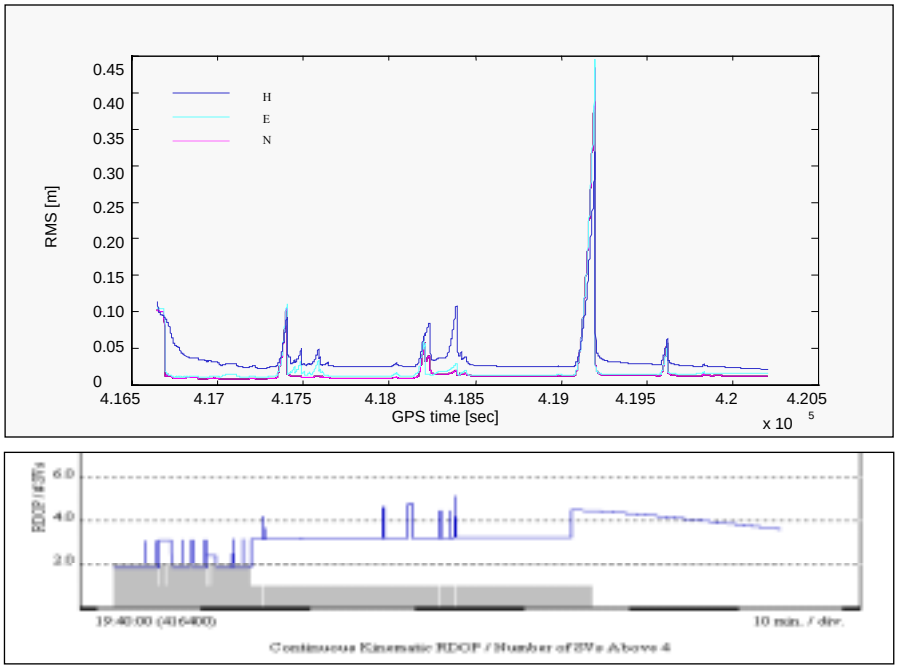

Figure 18. Position standard deviation and satellite observability for the entire test duration (land-based application).

The estimated standard deviations, normally achievable with this system under favorable GPS conditions, are at the level of 1-3 cm in horizontal coordinates (30-50% higher for the vertical component) for baselines up to 50-60 km, and 5-7 arcsec and ~10 arcsec for attitude and heading components, respectively (for extended losses of lock, above 60 s, errors in position can grow to 10-20 cm and more, depending on the gap size, see Section 8.3). For longer baselines, exceeding 100 km (usually airborne case), and under favorable GPS geometry (6-8 satellites), the standard deviations can reach 3-4 cm for horizontal and up to 4-6 cm for vertical coordinate; attitude standard deviations are functions of quality of GPS data used to calibrate the IMU sensors and the geometry of the trajectory (in general, long straight portions of the flight will cause heading error growth, while aircraft maneuvers allow for better sensor error decorrelation, and will bring the standard deviations significantly down (see Figure 20)).

A typical behavior of the positional and attitude standard deviations for this system is presented in Figures 18, 19 and 20. Figure 18 also presents the number of satellites tracked and the corresponding RDOP (Relative Dilution of Precision) values. Lower number of satellites and higher RDOP are immediately reflected in lower positioning accuracy, as can be observed in the figure. The spikes in the position standard deviation plot correspond to the partial or total losses of GPS lock when the vehicle was passing under the foliage or close to the buildings. The corresponding positional standard deviations for the airborne case (where losses of lock are rather infrequent) are presented in Figure 19.

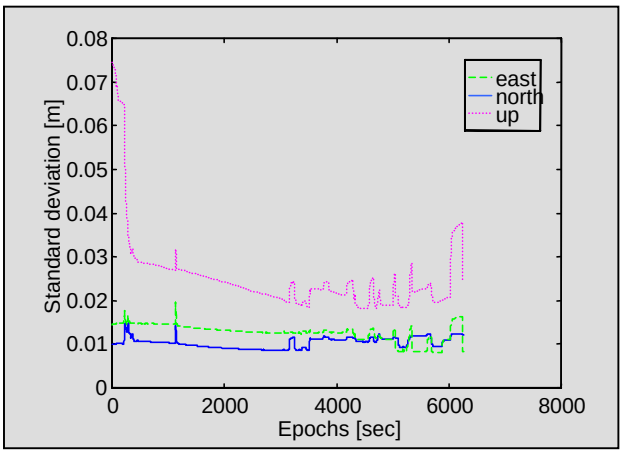

Figure 19. Estimated standard deviations for rover position (airborne application).

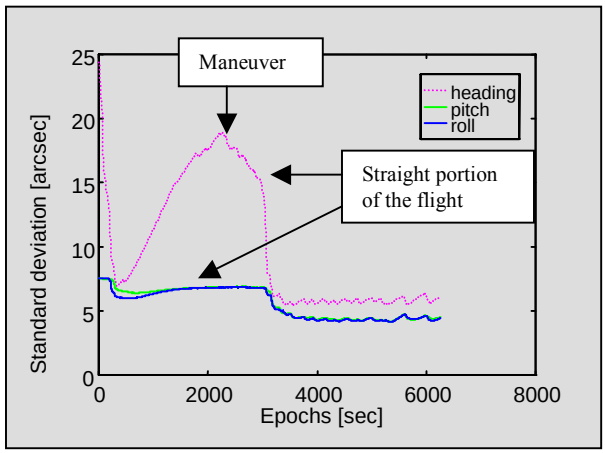

Figure 20. Estimated standard deviations for attitude (airborne application).

The same nominal accuracy, provided by the navigation component, will result in totally different positional object errors for various object distances, typical for airborne and land-based applications, as explained earlier. Thus, an ultimate performance assessment can be achieved by comparing the coordinates of ground control identified in the directly oriented imagery. Tables 9 and 10 below present a typical fit to ground truth for airborne and land-based cases, where object distance was ~300 m (ground pixel size of ~10 cm) and 8-18 m (ground pixel size of ~0.5 cm), respectively.

The analysis of the airborne test results (flight trajectory shown in Figure 21) indicates that they were significantly affected by mechanical problems with the camera body/mount (some flex between the camera and INS was present) and rather poor quality of the boresight transformation, which was performed based on natural features as opposed to the specialized targets, which resulted in rather moderate accuracy of the AT solution used to determine the boresight parameters (see Section 7.2 for more explanation on boresight calibration). The accuracy of AT attitude components was at the level of 0.3 – 1.5 arcmin, and the perspective center coordinates were estimated with the average accuracy of 0.04 – 0.14 m, translating (in conjunction with the mechanical problems mentioned) to the boresight accuracy of 0.29, 0.17 and 0.15 m for the linear displacements, and 3.7, 2.7 and 1.7 arcmin for the rotation angles, respectively (for the estimates based on the six centrally located images, containing the majority of the control points, the respective standard deviations were: 0.22, 0.08 and 0.06 m for the offsets, and 1.8, 2.4 and 0.6 arcmin for the rotation angles) (Grejner-Brzezinska, 1999).

On the other hand, the boresight accuracies achieved on a specialized range for the land-based test presented in Table 10 were 2-3 cm for linear offsets and 17-22 arcsec for angular offsets, respectively, resulting immediately in much better match to ground truth. Generally, a fit to ground truth at the level of 20-30 cm for airborne (~300 m object distance) (similar accuracies were also reported by Mostafa and Schwarz, 1999) and 1-3 cm for land-based applications (< 20 m object distance) was demonstrated with the GPS/INS prototype presented here. It is fair to expect that improvements in large scale AT used to derive the boresight transformation for airborne case would lead to significant improvements in DOP performance.

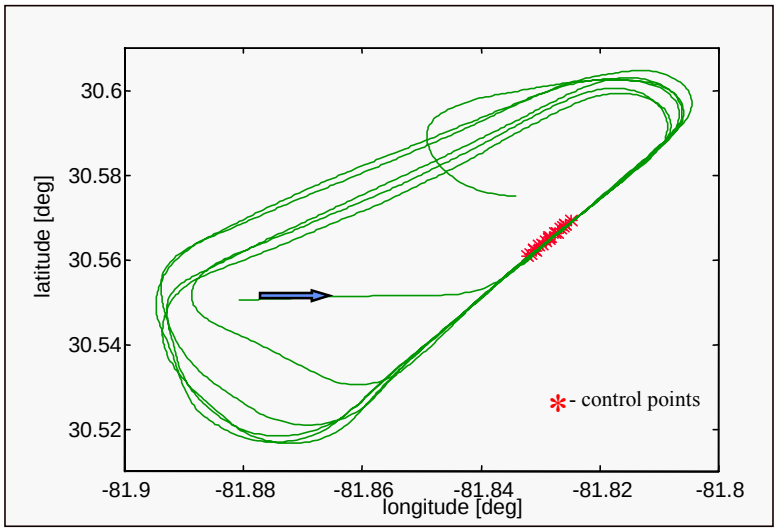

Figure 21. Aircraft trajectory over the Callahan area, June 2, 1998.

Table 9. Average differences between nominal and manually measured control point coordinates on directly oriented images, airborne application.

Stereo Pair		dX		dY		dZ	
		Average	**Sigma**	**Average**	**Sigma**	**Average**	**Sigma**
37425	37026	-0.132	0.193	-0.154	0.185	0.230	0.206
37026	36620	0.154	0.294	-0.189	0.188	0.442	0.158
36620	38274	0.159	0.095	-0.083	0.170	0.298	0.219
38274	37419	-0.271	0.514	0.292	0.140	-0.255	0.065
Total Average		0.034	0.311	-0.066	0.237	0.298	0.219
RMS		0.187		0.195		0.317	

Table 10. Coordinate difference for checkpoints, land-based application.

Point	Object distance	Easting [m]	Northing [m]	Height [m]
1	17.25	0.002	0.029	0.008
2	16.30	0.009	0.015	0.000
3	18.57	-0.019	0.029	0.010
4	17.86	-0.059	0.018	0.009
RMS		0.031	0.007	0.005

The overall accuracy measure can also be achieved by examining the repeatability of the solution obtained for the checkpoints measured on different directly oriented stereo pairs. The statistics of such a comparison, based on over 40 stereo pairs, collected in land-based application is presented in Table 11. Another repeatability test was performed by comparing the ground coordinates of 15 check points measured on the directly oriented stereo pairs from two different passes (the entire test trajectory consisted of 2 repeated tracks), also shown in Table 11. The GPS/INS/image data for the two passes were collected with slightly different GPS constellation; pass one observed six satellites, whereas pass two was able to collect GPS data from five and less

satellites. Still, the repeatability was achieved at 1-2 cm RMS level within the same pass, and at 2-5 cm level between the repeated passes.

Table 11. Ground coordinate difference for the check points measured from different stereo pairs (left side of the table) and for 15 check points measured on stereo pairs from overlapping passes (right side of the table).

Statistic	Easting [m]	Northing [m]	Height [m]	Statistic	Easting [m]	Northing [m]	Height [m]
Mean	0.015	0.004	0.008	**Mean**	0.015	0.014	0.044
Median	0.006	0.003	0.006	**Median**	0.013	0.011	0.045
Maximum	0.050	0.025	0.035	**Maximum**	0.050	0.034	0.130
RMS	0.019	0.007	0.010	**RMS**	0.020	0.018	0.052

8.3. What are the other important accuracy measures?

8.3.1. Impact of GPS gaps

The quality of INS bridging during the GPS gaps strongly depends of the quality of IMU sensors (low cost sensors would drift much faster, especially in the vertical channel), the extent of the gap itself, the dynamics of the trajectory, and also the duration of the sensor error calibration prior to the gap, as illustrated in Tables 12 and 13 below, for the LN-100 INS. The positioning errors listed in Table 12 are the differences between the reference GPS/INS solution and the INS only solution when GPS was turned off. In Table 13 the error is defined as a difference between the INS free navigation mode and the GPS/INS solution after the GPS lock was recovered.

For the tests presented in Table 12, the positioning standard deviations before the gap were 0.005, 0.01 and 0.05 m for Easting, Northing and Height, respectively, for the solution with 200-s calibration period, and 0.005, 0.007 and 0.02 m, respectively, for the solution with 600-s calibration period. As mentioned earlier, the dynamics (geometry) of the calibration period plays a significant role in the overall error growth during the gap, which is illustrated in Table 12: for example, a 200-s (1^{st}) and 600-s calibration periods were both performed under high dynamics (the vehicle was performing circles), thus sensor errors were reasonably well decorrelated in both cases; consequently the overall error growth is similar. The second test with a preceding 200-s calibration period shows much faster error growth due to the fact that the calibration was done during the straight portion of the trajectory. Similarly, the 84-s gap that follows a 236-s calibration period performed during the straight portion of the flight, as presented in Table 13, displays a relatively faster error growth during the gap, as compared to the error growth for a similar (200-s) calibration period (1^{st}) as presented in Table 12. Much longer gap, 140 s in duration, as presented in Table 13, preceded by a 723-s calibration period under varying geometry of the trajectory produces much smaller errors as compared to a shorter gap of 84 s with a shorter calibration period.

Table 12. Quality of INS bridging during the GPS gap (simulated gaps in GPS data).

Calibration period [s]	Total error [m]								
	60 second gap			120 second gap			180 second gap		
	East	North	Height	East	North	Height	East	North	Height
200	0.07	0.08	0.10	0.27	0.28	0.28	0.65	0.67	0.62
600	0.07	0.08	0.10	0.30	0.32	0.32	0.74	0.76	0.72
200 (straight part of the trajectory)	0.15	0.19	0.17	0.48	0.56	0.41	0.85	0.92	0.68

Table 13. Quality of INS bridging during the GPS gap (real gaps experienced during the flight)

	East	North	Height
Total error [m]	0.19	0.40	0.58
Gap duration [sec]	84		
INS calibration [sec]	236		
Total error [m]	0.12	0.06	0.18
Gap duration [sec]	140		
INS calibration [sec]	723		

8.3.2. Effect of the quality of gravity compensation

Since INS needs gravity compensation to navigate (as explained in Section 5.1), the better the gravity information (model) used, the better positioning quality should be. Different models, ranging from the normal gravity to high order spherical harmonic expansion, can be used to approximate the Earth's gravity field. The normal gravity model approximates the Earth's gravitation with an accuracy of 1 part in 10^4, whereas detailed global gravitational models are good to 1 part in 10^5. Most commonly, normal gravity model is used in the inertial navigation algorithm, but if higher order spherical harmonic expansion were used for computing the gravity intensity for the vertical axis in the navigation algorithm, the better the accuracy of the vertical velocity and altitude determination should be expected. Consequently, since the velocity error couples from the vertical to horizontal axes (and vice versa) through the error in the Coriolis term, these effects are reduced as the velocity error is reduced due to less error from the gravity anomaly vector. Moreover, when the deflections of the vertical are compensated, there is less tilt error, and consequently, less coupling of the horizontal accelerations into the vertical axis. Thus, it can be expected that (high-accuracy) deflection of the vertical (DOV) compensation should improve not only the positioning accuracy, but also the attitude determination of the platform. This can be verified by close examination of the dynamics matrix of the system, which shows the interrelation among the estimated errors. The errors in DOV enter directly into the horizontal

velocity errors in linear combination with the attitude errors. This, generally speaking, complicates full separation in the estimation procedure. However, if one of the components, in this case DOV, becomes (partially) known, an improvement in estimation of the attitude should ultimately be achieved (see Grejner-Brzezinska and Wang, 1998, for more details).

In the example presented here, the unclassified NIMA Standard Inertial Navigation Product (INP) was used over the designated test areas. INP is a three-dimensional, gridded database of DOV and their errors at 2'×2' separation ranging from 0 ft to 90K ft above the geoid level. The accuracy of the gravity anomaly ranges between 1 and 5 mgal (5 mgal corresponds roughly to 1 arcsec in deflection accuracy).

As can be observed in Table 14, the improved positioning accuracy is achieved during the GPS losses of lock if DOV compensation is applied in the strapdown navigation algorithm. In addition, a decrease in the estimated standard deviations of the attitude components by 1.5-2.5 arcsec with respect to the case where no DOV compensation was used was also achieved (see Grejner-Brzezinska and Wang, 1998 for more details). This represents an average gain due to the DOV compensation, and is observed at a similar level for all the analyzed test flights (average altitude of 4500 and speed of 125 m/s) (see Table 15). In general, the amount of DOV compensation applied (1-5 arcsec on average) is reflected in the order of magnitude of the attitude differences between both solutions, as shown in Table 15. Moreover, some improvements in the order of 1 arcsec (average) for the heading standard deviation were observed. Generally, the DOV-compensated solution shows faster convergence and steadier spectrum of the standard deviation, as compared to the uncompensated mode.

Table 14. Errors in horizontal coordinates after 60-second GPS gap (after a 15-min calibration period). Error is defined as a difference between a reference GPS/INS solution and the solution where GPS was turned off for 60 s.

Horizontal Coordinate	Solution without DOV		Solution with DOV	
	Error [m]	Positional sigma [m]	Error [m]	Positional sigma [m]
East	**0.03**	**0.10**	**0.02**	**0.08**
North	**0.07**	**0.12**	**0.03**	**0.10**

Table 15. Difference in attitude between solutions with and without DOV compensation.

Tilt	Flight #	RMS [arcsec]	Max [arcsec]	Mean [arcsec]
Pitch	1	3.9	10.9	1.7
	2	3.0	8.4	-0.1
	3	5.6	12.2	-1.6
Roll	1	3.3	11.1	-0.8
	2	3.1	11.1	-0.4
	3	4.0	12.1	2.7

5. FUTURE TRENDS

In the previous sections the current level of development and achievable accuracy of modern mobile mapping systems were presented. The expansion of the technology in the recent years was demonstrated, and thus it is rather safe to predict that this trend will continue in the coming years. The proliferation of GPS/INS, improvement in CCD technology as well as expected price drop of these systems should make MMS even more attractive to GIS, mapping and remote sensing community. The MMS community is quite sizable and continues to grow; this can be concluded from the number of participants of the International Mobile Mapping Symposia, as well as the number of systems presented at these meetings (so far three such meetings have been held: in 1995, at the Center for Mapping, Columbus OH, in 1998, in Bangkok Thailand, and in January 2001 in Cairo Egypt). Interested readers are referred to the Conference Proceedings, which provide numerous publications describing new MMS in both land and airborne applications, technological advancements, sensor development, new methods of data flow automation and feature extraction, etc. (see Reference section under "Proceedings").

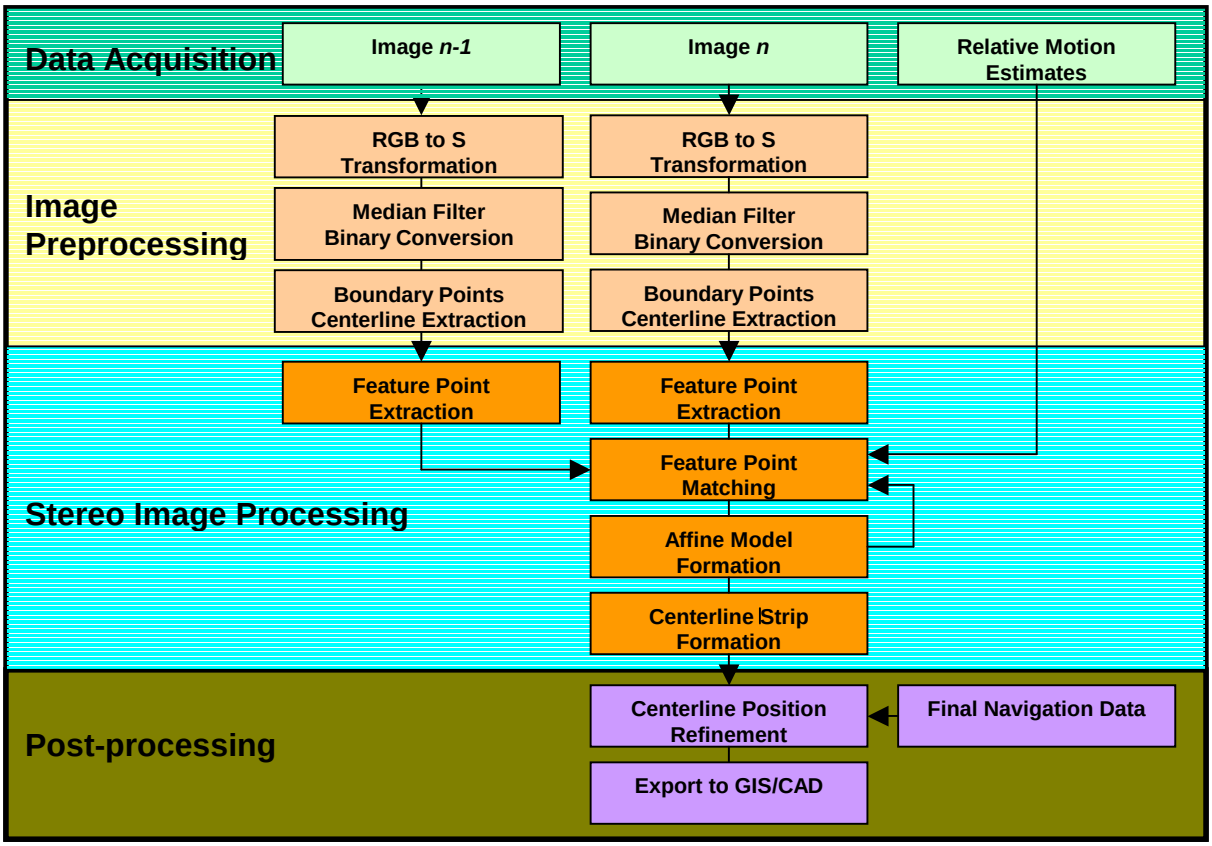

Figure 22. Real-time and post-processing modes of image/navigation data processing in MMS.

The expected major trends for the nearest future are the increase in real-time image processing, expansion of the intelligent features of MMS (sophisticated on-the-fly quality assurance modules,

more ITS[2]-oriented and automated machine navigation applications, etc; see for example, Kahmen and Retscher, 1999) and automation of data processing, as well as development of multi-sensor imaging systems (see, for example Cramer et al., 1999; El-Sheimy and Schwarz, 1999; Fuse and Shimizu, 1999; Li et al., 1999; Savopol et al, 2000; Tao et al., 1999; Toth and Grejner-Brzezinska, 1999 and 2000). Figure 22 presents an example of real-time and post-processing image and navigation data flow for a Mobile Mapping system currently under development at The Ohio State University. The simple sensor assembly (single down-looking camera) and a rather uncomplicated and predictable object contents of the images – center or edge lines of the road – enable a significant amount of real-time image pre-processing (Toth and Grejner-Brzezinska, 2000). It is expected that real-time processing and QC modules as well as automated data flow will further shorten the production cycle, minimize the human interaction, and will consequently enable an easy transfer of Mobile Mapping technology to other platforms and applications.

10. SUMMARY

In this contribution, a brief history of the past ten years of modern Mobile Mapping technology is presented with a special emphasis on the system design, implementation and operational aspects, including the inertial navigation concept, GPS/INS integration scheme and short introduction to modern imaging sensors used in land MMS and airborne remote sensing, based on GPS/INS fusion. The detailed discussion of DPO by means of GPS/INS, including its benefits and drawbacks, integrated system calibration, currently achievable accuracy and example systems implemented to date are also presented. A special emphasis is put on the GPS/INS navigation component that enabled the MMS technology, and whose further improvements over the years allowed the extension of this technology to, even more challenging, DPO-based airborne mapping. The technology significantly evolved since its inception in late 1980s and early 1990, expanding its market from rudimentary land-based mapping applications to more sophisticated multi-sensor airborne systems. Automation and increase in real-time operations are the current and future trends, which should enable further expansion of MMS technology to ITS and machine navigation markets. Existing literature review is provided for further reference.

[2] Intelligent Transportation Systems

Appendix A: System Dynamics

Detailed expression for sub-matrices F_{1j} ($j=1,2,3,4$) and F_{22} of the dynamics matrix F from Equation (5):

$$F_{11}=\begin{bmatrix} 0 & -\dot{\lambda}sL & \dot{L} & 1 & 0 & 0 & 0 & 0 & 0 \\ \dot{\lambda}sL & 0 & \dot{\lambda}cL & 0 & 1 & 0 & 0 & 0 & 0 \\ -\dot{L} & -\dot{\lambda}cL & 0 & 0 & 0 & 1 & 0 & 0 & 0 \\ -\frac{g}{R_e} & 0 & 0 & 0 & -(2\omega_{ie}+\dot{\lambda})sL & \dot{L} & 0 & -f_D & f_E \\ 0 & -\frac{g}{R_e} & 0 & (2\omega_{ie}+\dot{\lambda})sL & 0 & (2\omega_{ie}+\dot{\lambda})cL & f_D & 0 & -f_N \\ 0 & 0 & \frac{2g}{R_e} & -\dot{L} & -(2\omega_{ie}+\dot{\lambda})cL & 0 & -f_E & f_N & 0 \\ 0 & 0 & 0 & 0 & 0 & 0 & 0 & -(\omega_{ie}+\dot{\lambda})sL & \dot{L} \\ 0 & 0 & 0 & 0 & 0 & 0 & (\omega_{ie}+\dot{\lambda})sL & 0 & -(\omega_{ie}+\dot{\lambda})sL \\ 0 & 0 & 0 & 0 & 0 & 0 & -\dot{L} & (\omega_{ie}+\dot{\lambda})sL & 0 \end{bmatrix} \quad (A1)$$

where

$(sL=\sin(L),\ cL=\cos(L))$

$$F_{12}=I(3\times 3) \qquad (A2)$$

$$F_{13}=\begin{bmatrix} 0(3\times 3) & 0(3\times 3) \\ C_b^n & C_b^n\begin{bmatrix} f_x & 0 & 0 \\ 0 & f_y & 0 \\ 0 & 0 & f_z \end{bmatrix} \\ 0(3\times 3) & 0(3\times 3) \end{bmatrix} \qquad (A3)$$

$$F_{14}=\begin{bmatrix} 0(6\times 3) & 0(6\times 3) \\ -C_b^n & -C_b^n\begin{bmatrix} \omega_x & 0 & 0 \\ 0 & \omega_y & 0 \\ 0 & 0 & \omega_z \end{bmatrix} \end{bmatrix} \qquad (A4)$$

$$F_{22}=diag\begin{bmatrix} -\tau_{gN} & -\tau_{gE} & -\tau_{gD} \end{bmatrix} \qquad (A5)$$

In the equations above C_b^n is the direction cosine matrix from body-fixed frame (*b*-frame) to navigation frame (*n*-frame), ω_{ie} is the Earth's rotation rate, L is the geodetic latitude, and λ is the geodetic longitude, g is the gravity constant, (f_x, f_y, f_z) is the accelerometer sensed specific force vector defined in the *b*-frame, (f_N, f_E, f_D) is the same specific force vector coordinatized in the *b*-frame, $(\omega_x, \omega_y, \omega_z)$ is the gyro sensed vehicle rotation rate vector. R_e equals the Earth radius plus vehicle altitude, and τ_g is the time constant for the Markov processes of gravity uncertainties.

REFERENCES

Abdullah, Q., (1997): Evaluation of GPS-Inertial Navigation System for Airborne Photogrammetry, presented at 1997 ACSM/ASPRS Annual Convention and Exposition, April 7-10, Seattle, WA.

Arshal, G. (1987): Error Equations of Inertial Systems, *Journal of Guidance, Navigation and Dynamics*, Vol. 10, No. 4, pp. 351-358.

Axelsson, P., (1999): Processing of Laser Scanner data – Algorithms and Applications, ISPRS Journal of Photogrammetry and Remote Sensing No. 54, pp.138-147.

Bar-Itzhack, I. Y. and Berman, N. (1988): Control Theoretic Approach to Inertial Navigation Systems, *AIAA Journal of Guidance, Control, and Dynamics*, Vol.11, No.3, pp. 237-245.

Bossler, J. D., Goad, C., Johnson, P., and Novak, K., (1991): GPS and GIS Map the Nation's Highway, *GeoInfo System Magazine*, March, pp. 26-37.

Bossler, J. D. and Novak, K., (1993): Mobile Mapping System: New Tools for the Fast Collection of GIS Information, Proc. GIS'93, Ottawa, Canada, pp. 306-315.

Bossler, J. D., and Toth, C., (1995): Accuracies Obtained by the GPSVan™, Proc. GIS/LIS'95, Vol. 1., pp. 70-77.

Bossler, J. D., and Schmidley, R. W. (1997): Airborne Integrated Mapping System Promises Large-Scale Mapping Advancements, *GIS World*, Vol. 10, No. 6, pp. 46-48.

Britting, K. R. (1971): *Inertial Navigation Systems Analysis*, Wiley-Interscience, a Division of John Wiley and Sons, Inc.

Bruce, M. (1998): An ultra high resolution, electro-optical framing camera for reconnaissance and other applications using a 9126 by 9126 pixel, wafer scale, focal plane array. Proc. SPIE Conference on Airborne Reconnaissance XXII, Vol. 3431, pp. 144-154.

Cramer, M, Stallmann, D. and Haala, N. (1999): sensor Integration and Calibration of Digital Airborne Three-line Camera Systems, Proceedings, International Workshop on Mobile Mapping Technology, Bangkok, Thailand, April 21-23, pp. 4-5-1 – 4-5-8.

Da, R., (1997): Investigation of Low-Cost and High-Accuracy GPS/IMU System, Proc. ION National Technical Meeting, Santa Monica, pp. 955-963.

Diener, S., Kiefner, M and Dorstel, C., (2000): Radiometric Normalization and Color Composite Generation of the DMC, International Archives of Photogrammetry and Remote Sensing, Vol. XXXIII, Part B1, CD ROM.

El-Sheimy, N., Schwarz, K. P., Gravel, M. (1995): Mobile 3-D Positioning Using GPS/INS/Video Cameras, Proc. Mobile Mapping Symposium, OSU Center for Mapping, pp. 236-249.

El-Sheimy, N. and Schwarz, K. P., (1999): Navigating Urban Areas by VISAT – A Mobile Mapping System Integrating GPS/INS/Digital Cameras for GIS Application, *Navigation*, Vol. 45, No. 4, pp. 275-286.

Flood, M., (1999): Commercial Development of Airborne Laser Altimetry, International Archives of Photogrammetry and Remote Sensing, Vol. 32, Part 3-W14, pp. 13-21.

Fuse, T and Shimizu, E., (1999): A Comparative Study on Techniques for Optical Flow Estimation: On the Application to Vehicle Motion Analysis, Proceedings, International Workshop on Mobile Mapping Technology, Bangkok, Thailand, April 21-23, pp. P2-7-1 – P2-7-6.

Gajdamowicz, K. and Ohman, D. (1998): Automatic Recognition and Positioning of Road Signals from Color Stereo Image Sequences, Object Recognition and Scene Classification from Multispectral and Multisensor Pixels, ISPRS Commission III Symposium, Columbus OH, pp. 218-224.

Goshen-Meskin, D. and Bar-Itzhack, I. Y. (1992): Unified approach to inertial navigation system error modeling, *AIAA Guidance, Control, and Dynamics*, Vol.15, No.3, pp. 648-653.

Greenspan, R. L. (1996): GPS and Inertial Integration, Chapter 7 in *Global Positioning System: Theory and Applications*, Vol. II, pp. 187-220, Parkinson, B. W. and Spilker, J. J. (ed), American Institute of Aeronautics and Astronautics, Inc.

Grejner-Brzezinska, D. A., (1996): Positioning Accuracy of the GPSVan™, Proc. 52nd ION Annul Meeting, pp. 657-665. Grejner-Brzezinska, D. A., (1997): Airborne Integrated Mapping System: Positioning Component, Proc. 53rd ION Annual Meeting, Albuquerque, NM, pp. 225-235.

Grejner-Brzezinska D. A (1999): Direct Exterior Orientation of Airborne Imagery with GPS/INS System: Performance Analysis, *Navigation*, Vol. 46, No. 4, pp. 261-270.

Grejner-Brzezinska D. A., Phuyal B. P., (1998): Positioning Accuracy of the Airborne Integrated Mapping System, Proc. ION Technical Meeting, Long Beach, CA, pp. 713-721.

Grejner-Brzezinska D. A. and Wang J. (1998): Gravity Modeling for High-Accuracy GPS/INS Integration, *Navigation*, Vol. 45, No. 3, pp.209-220.

Grejner-Brzezinska D. A., Da, R., Toth C., (1998): GPS Error Modeling and OTF Ambiguity Resolution for High-Accuracy GPS/INS Integrated System, *Journal of Geodesy*, 72(11), pp. 628-638.

Grejner-Brzezinska D. and Toth C. (2000a): Precision Mapping of Highway Linear Features, Geoinformation for All, Proceedings, XIXth ISPRS Congress, July 16-23 Amsterdam, Netherlands, pp. 233-240.

Grejner-Brzezinska D. and Toth C. (2000b): Real-time Tracking of Highway Linear Features, Proc. ION GPS, September 19-21, Salt Lake City, Utah, CD ROM.

He, G.P., Novak, K., and Tang, W. (1994): The Accuracy of Features Positioned with the GPSVan, Symp. ISPRS Comm. II Symposium, Vol. 30, Part 2, pp. 480-486.

Huddle, J. R. (1983): Inertial Navigation System Error Model Considerations in Kalman Filter Applications, C*ontrol and Dynamic Systems* (ed. C. T. Leondes), Vol. 20, No.2, pp. 294-340.

Kahmen, H. and Retscher, G. (1999): Precise 3-D Navigation of Construction Machine Platforms, Proceedings, International Workshop on Mobile Mapping Technology, Bangkok, Thailand, April 21-23, pp. 5A-2-1 – 5A-2-5.

Kerr III, T. (1994): Use of GPS/INS in the Design of Airborne Multi-sensor Data Collection Mission (for Tuning NN-based ATR Algorithms), PROC. ION GPS, Salt Lake City, Utah, pp.1173-1188.

Lachapelle, G., Lu, G., and Loncarevic, B., (1994): Precise Shipborne Attitude Determination Using Wide Antenna Spacing, PROC. KIS94.

Li D., Zhong, S., He, S. and Zheng, H. (1999): A Mobile Mapping System Based on GPS, GIS and Multi-sensor, Proceedings, International Workshop on Mobile Mapping Technology, Bangkok, Thailand, April 21-23, pp. 1-3-1 – 1-3-5.

Lithopoulos, E., Reid, B., Scherzinger, B., (1996): *The Position and Orientation System (POS) for Survey Applications*, International Archives of Photogrammetry and Remote Sensing, ISPRS Comm. III, Vol. XXXI, part B3, pp. 467-471.

May, M. B., (1993): Inertial Navigation and GPS, *GPS World*, September, pp. 56-66.

Mostafa, M., and Schwarz, K.P., (1999): A GPS/INS /Imaging System for Kinematic Mapping in Fully Digital Mode, *Geodesy Beyond 2000*, The challenges for the First Decade, IAG Symposia, Vol. 121, K. P. Schwarz (ed), Springer, pp. 331-336.

Novak, K. and Bossler, J. D., (1995): Development and Application of the Highway Mapping System of Ohio State University, Photogrammetric Record, 15(85), pp. 123-134.

Pfister, W., J. Steele, M. Farrier, C. Smith (1998): Fifty-Megapixel CCD Image Sensor With Motion Compensation. Proc. SPIE Conference on Airborne Reconnaissance XXII, Vol. 3431, pp. 161-169.

Proceedings, (1995) Mobile Mapping Symposium, The Ohio State University Center for Mapping.

Proceedings, (1999) International Workshop on Mobile Mapping Technology, Bangkok, Thailand, R. Li and S. Murai (ed).

Proceedings, (2001) The 3rd International Symposium on Mobile Mapping Technology, Cairo, Egypt.

Robson, S., M.R. Shortis (1998): Practical Influences of Geometric and Radiometric Image Quality Provided by Different Digital Camera Systems. Photogrammetric Record, 16(92), pp. 225-247.

Reulke, R., Franke, K-H., Fricker, P., Pomierski, T., Sandau, R., von Schonermark, M., Tornow, C. and Wiest, L., (2000): Target Related Multispectral and True Color Optimization of the Color Channels of the LH Systems ADS40, International Archives of Photogrammetry and Remote Sensing, Vol. XXXIII, Part B1, CD ROM.

Savopol, F., Chapman, M. and Boulianne, M., (2000): A Digital Multi CCD Camera System for Near Real-Time Mapping, Proceedings, XIXth ISPRS Congress, July 16-23 Amsterdam, Netherlands, pp. 266-271

Sandau, R., Braunecker, B., Driescher, H., Eckardt, A., Hilbert, S., Hutton, J., Kirchhofer, W., Lithopoulos, E., Reulke, R. and Wicki, S., (2000): design Principles of the LH Systems ADS40 Airborne Digital Sensor, International Archives of Photogrammetry and Remote Sensing, Vol. XXXIII, Part B1, CD ROM.

Skaloud, J., Cramer, M., Schwarz, K.P., (1996): Exterior Orientation by Direct Measurement of Camera Position and Attitude, International Archives of Photogrammetry and Remote Sensing, Vol. XXXI, Part B3, pp. 125-130.

Schwarz, K. P., Chapman, M., Cannon, M. E., and Gong, P., (1993): An Integrated INS/GPS Approach to the Georeferencing of Remotely Sensed Data, PE&RS Vol. 59, No. 11, pp. 1667-1674.

Schwarz, K. P., Wei, M., (1994): Aided Versus Embedded A Comparison of Two Approaches to GPS/INS Integration, Proceedings of IEEE Position Location and Navigation Symposium, Las Vegas, NE, pp. 314-321.

Siouris, G. M., (1993): *Aerospace Avionics Systems*, Academic Press, Inc.

Tao, C., Chapman, M., El-Sheimy, N. and Chaplin (1999): Towards Automated Processing of Mobile Mapping Image Sequences, Proceedings, International Workshop on Mobile Mapping Technology, Bangkok, Thailand, April 21-23, pp. 2-3-1 – 2-3-9.

Toth, C., (1995a): Experiences with a Fully Digital Image Acquisition System, Proc. ASPRS-ACSM Annual Convention, Vol. 2, pp. 18-24.

Toth, C., (1995b): A Conceptual Approach to Imaging for Mobile Mapping, Proceedings Mobile Mapping Symposium, OSU, pp. 19-27.

Toth, C. K., (1998): Airborne Experiences with a 4K by 4K CCD Sensor, Proc. ASPRS-ACSM Annual Convention, CD-ROM, pp. 163-168.

Toth C. K. (1999): Experiences with Frame CCD Arrays and Direct Georeferencing, Photogrammetric Week 99, pp. 95-107, Fritsch and Spiller (Editors), Wichmann Verlag.

Toth C. and Grejner-Brzezinska D. (1999): Improved DEM Extraction Techniques – Combining LIDAR Data with Direct Digital GPS/INS Oriented Imagery, Proceedings, International Workshop on Mobile Mapping Technology, Bangkok, Thailand, April 21-23, pp. 6A-4-1 – 6A-4-7.

Toth C. and Grejner-Brzezinska D. (2000): Complementarity of LIDAR and Stereo-imagery for Enhanced Surface Extraction, Geoinformation for All, Proceedings, XIXth ISPRS Congress, July 16-23 Amsterdam, Netherlands, pp. 897-904.

Ward, L., Axelrad, P., *A*., (1997): Combined Filter for GPS-based Attitude and Baseline Determination, Navigation, Vol. 44, pp.195-213.

Wehr A. and Lohr U., (1999): Airborne Laser Scanning – and Introduction and Overview, ISPRS Journal of Photogrammetry and Remote Sensing No. 54, pp.68-82.